T E C H N I S C H E U N I V E R S I T Ä T M Ü N C H E N

Institut für diagnostische und interventionelle Radiologie
am Klinikum rechts der Isar
(Direktor: Univ.-Prof. Dr. E. J. Rummeny)

Monitoring of New Immunotherapies for Prostate Cancer with Optical Imaging

Verena Christina Reinhart

Vollständiger Abdruck der von der Fakultät für Medizin der Technischen Universität München zur Erlangung des akademischen Grades eines

Doktors der Medizin

genehmigten Dissertation.

Vorsitzender: Univ.-Prof. Dr. P. Henningsen

Prüfer der Dissertation:

1. Univ.-Prof. Dr. E. J. Rummeny
2. Univ.-Prof. V. Ntziachristos, Ph.D.

Die Dissertation wurde am 02.11.2012 bei der Technischen Universität München eingereicht und durch die Fakultät für Medizin am 17.07.2013 angenommen.

Index

1 Introduction

The incidence of prostate cancer in the United States is 230,000 cases per year causing 30,000 deaths annually. Therefore it is the second leading cause of cancer-related death [7, 22, 53]. The treatment concept of hormone therapy by deprivation of androgens can obtain temporary regression or gain control of metastases of prostate cancer. However, the frequently occurring hormone-refractory disease is a feared consequence of the hormone treatment concept as this disease is difficult to control and impossible to cure with current chemotherapy. For this reason new treatment strategies are required and lead to new immunotherapies against prostate cancer which recently provided promising results [7, 22, 53, 58, 77]. The high and selective cytotoxicity of natural killer (NK) cells against cancer cells is a new therapeutic approach which seeks to avoid harming healthy cells [22, 58, 77]. There are two options for the application of NK cells for cancer therapy: either endogenous NK cells are activated through systemic administration of cytokines or ex vivo expanded and activated autologous or donor-derived NK cells are transferred by adoptive therapy for which clinical applicable NK cells are needed [30, 40, 48, 77, 84, 106, 121]. Phase I and II clinical trials have been initiated as NK cells provide a high intrinsic cytotoxic activity against various malignancies without demonstrating toxicity [27, 54, 96, 106].

At present the efficacy of NK cell therapy in patients is quantified indirectly through the level of tumor markers and survival of patients. PCR (polymerase chain reaction) is used to evidence that a significant amount of NK cells departs the blood circulation within minutes after application. Clinically the accumulation of NK cells in the tumor is difficult to prove as mostly a combination of cytotoxic drugs and NK cells is administered [27, 54, 96, 106].

In order to confirm the tumor response to the NK cell therapy, new molecular imaging techniques have to be applied for monitoring the accumulation of NK cells through noninvasive in vivo cell tracking of NK cells in the tumor [18, 20, 21]. NK cell tumor accumulation and its cytotoxic activity could be further examined by using in vivo NK cell tracking techniques. Different techniques can be used for tracking NK cells: single-photon emission computed tomography (SPECT), positron emission tomography (PET), optical imaging (OI) and magnetic resonance imaging (MRI) [2, 31, 65]. The imaging technique applied for this thesis is OI which demonstrates several advantages compared to other imaging techniques: the absence of radiation exposure, high sensitivity, fast and simple data acquisition and the inexpensive application [19, 74].

The objectives of this thesis were:

1) To label parental NK cells and genetically modified NK-92-scFv(MOC31)-ζ, NK-92-scFv(FRP5)-mζ and NK-92-scFv(FRP5)-ζ cells with iron oxides or fluorophores
2) In vitro: to obtain quantitative data concerning the characteristics and cytotoxicity of iron oxide labeled and unlabeled parental NK cells or genetically modified NK-92-scFv(MOC31)-ζ, NK-92-scFv(FRP5)-mζ and NK-92-scFv(FRP5)-ζ cells against the prostate cancer cell lines DU-145, LnCAP and PC-3 or against the breast cancer cells lines MDAMB-453 and MCF-7.
3) In vivo: to track the migration, homing and accumulation of fluorophore labeled NK-92-scFv(MOC31)-ζ cells injected into the tail vein of the rats to the implanted human prostate tumors (DU-145) with optical imaging.

2 Background

2.1 Adoptive Immunotherapies for the Treatment of Prostate Cancer

2.1.1 Overview

Prostate cancer is the most frequently diagnosed malignancy of men in Europe, North America and Africa. Worldwide, the incidence in 2002 was estimated to be half a million, representing almost 10 % of all malignancies in men. In the United States, prostate cancer is the most frequent cancer besides skin-cancer and the second leading cause of cancer deaths [38, 82, 90]. Therefore new therapies are being researched. Adoptive immunotherapy is an innovative and promising approach in the treatment of cancer and is based on the idea of destroying malignancy by a stimulated immune system. Immunotherapy with NK cells can be performed by activation of endogenous NK cells through systemic application of cytokines or by adoptive transfer of ex vivo expanded and activated autologous or donor derived NK cells. Under the former approach, a patient's lymphocytes are removed and stimulated by thymus peptides, cytokines as well as bacterial substances. The lymphocytes, which are increased in their immune capability, are transferred back into the patient. If the antigen of the tumor is established, specific activated T cells or monoclonal specific antibodies can be detected. The latter approach includes the use of cytotoxic NK cell lines that are suitable for clinical use. The continuously growing NK-92 cell line is characterized by a highly homogenous effector cell population, a well defined target specificity, lack of inhibitory NK cell receptors, highly effective cytotoxicity against malignant cells of hematologic origin and low toxicity against non-malignant cells. The NK-92 cell line is one of the few NK

cell lines which shows promising results in initial clinical trials [110]. In order to expand the selective, high cytotoxicity of NK-92 cells, genetically modified NK-92 cells have been developed which stably express a specific chimeric antigen receptor against the EpCAM antigen. The EpCAM antigen is overexpressed in prostate cancer and can be used as a target for a specific immunotherapy with EpCAM targeted NK cells [80].

2.1.2 NK Cell Therapies

Natural killer (NK) cells belong to the group of lymphocytes and constitute a major component of the innate immune system. They have the ability to kill abnormal cells, such as virus-infected and malignant cells, by dispensing perforin and granzym that effect apoptosis. NK cells do not express T-cell antigen receptors or rearrange their immune receptor genes. It is known that NK cells are activated with cytokines, above all interleukin-2, but do not develop markers of major histocompatibility complex on the cell surface. Sensitization is not required for the cells to be cytotoxicly activated [110]. The continuously growing natural killer cell line NK-92 was developed in 1992 by isolating peripheral blood lymphocytes of a patient with large granular lymphoma [106]. NK-92 cells exhibit high cytotoxicity against a diversity of malignancies in vitro and in mouse models in vivo, as well as interleukin-2 (IL-2) dependency. [110].

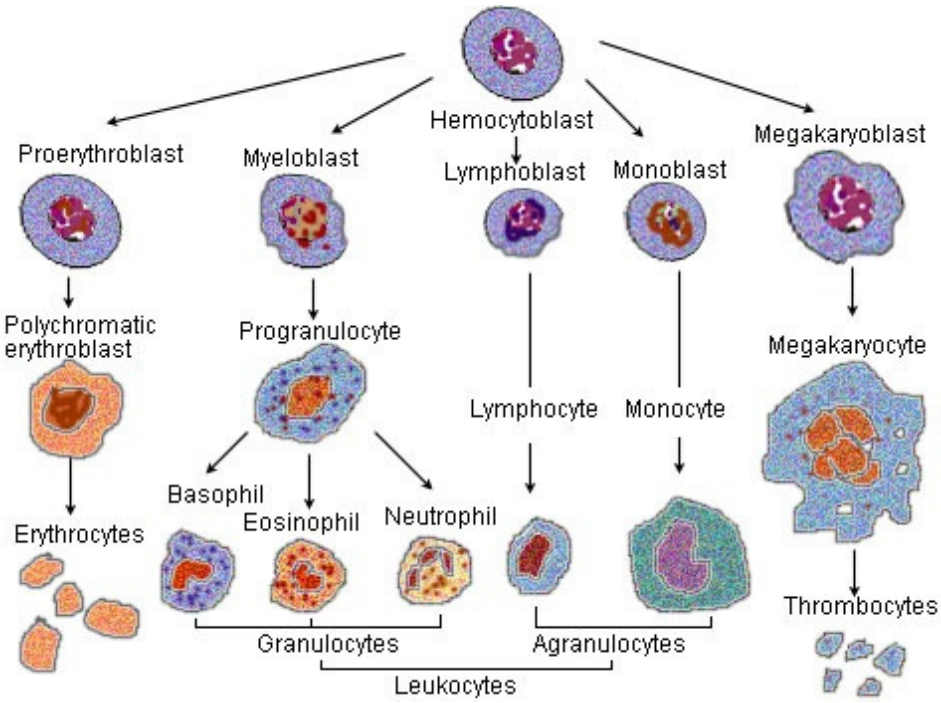

Fig. 2.1: Hematopoiesis in humans [11]

Furthermore they resemble activated killer cells (A-NK) in regard to surface receptor expression and functional characteristics. NK-92 cells exhibit higher cytotoxicity than A-NK cells against an expanded spectrum of malignancies. This advantage is explained by the fact that inhibiting NK cell receptors (NKRs), especially killer cell immunoglobin-like receptors (KIRs) are lacking the NK-92 cells. However, the outstanding benefit of the NK-92 cell line over the A-NK cells is the non-toxicity against nonmalignant allogeneic cells [110]. The high cytotoxic activity mediated by perforin and granzym is amplified by establishing genetically modified NK-92 cells. These cells express chimeric antigen receptors that are specific for the tumor-associated EpCAM antigen. [109]. There are challenges including the risk to graft in immune compromised patients, the risk to induce secondary lymphoma, potential dysfunctions in the NK cell populations with metastasis of tumor cells and the development of mechanisms to escape NK cell immunosurveillance through the tumor [106]. However, the rapid cytolytic action and the broad target range are promising for cancer therapy to target a large variety of malignancies [88]. Several studies have been conducted to improve the antitumor effect of NK cells through

endogenous activation of the patients' cells by applying cytokines or by using ex-vivo expanded autologous or donor derived cells. The NK-92 cell line is the only cell line besides TALL-104 that has been developed continuously for adoptive immunotherapy and has entered clinical trials [106].

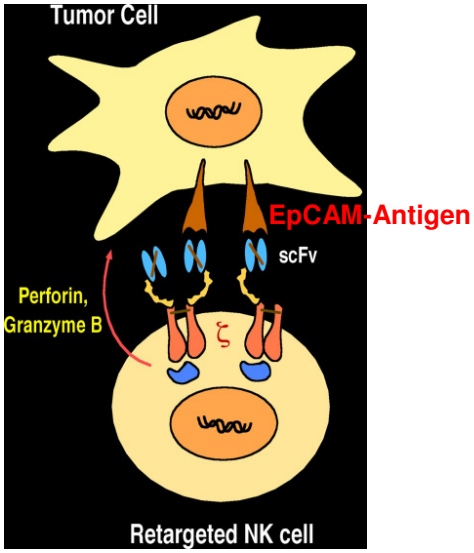

Fig. 2.2: Principle of retargeted NK cells

2.2 Labeling of NK Cells

2.2.1 Optical Imaging

2.2.1.1 Fluorescent Dyes

Intrinsic Dyes	Extrinsic Dyes			
	targeted	non-targeted	colloidal quantum dots	bifunctional label
- green fluorescent protein - red fluorescent protein	- simple targeting - cross-linking - enzyme activable	- ICG - DiI - DiO - DiD	- CdSe - CdTe - ZnS	- gadolinium-rhodamine nanoparticles - gadophrin-2 - gadofluorine-Cy-3

Tab. 2.1: Fluorescent Dyes

Fluorescent dyes can be divided into intrinsic and extrinsic labels. Intrinsic labels comprise fluorescent proteins in the cells, which require no substrate, have a high signal-to-noise ratio, are non-toxic, stable at 37° and resistant to photobleaching [39]. An example of intrinsic probes is the green fluorescent protein (GFP)[75] which is depicted in fig. 2.3.

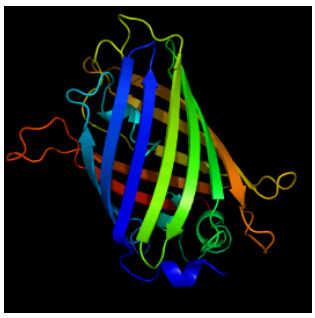

Fig. 2.3: GFP ribbon diagram [75]

This protein which comprises 238 AS was isolated from the jellyfish Aequorea Victoria in 1961 and fluoresces green when it is exposed to blue light. The GFP gene is labeled intrinsic as it can be introduced into the genome of organisms. A viral vector can be used to introduce the gene by local injection [92]. GFP is a sensitive marker that can be detected with fluorescence microscopy, flow cytometry and optical imaging. Its native protein is fluorescent in living cells. Hence, it can be implemented in situ detections in living animals [124]. Since the isolation of GFP, many different GFP-like proteins have been discovered, such as monomeric red, orange and yellow fluorescent proteins [94, 95]. Monomeric red fluorescent protein seems best suited to improve fluorescent protein in vivo application because of its somatic hypermutation and consequently its photostability and far-red emission, which allows for better tissue penetration [113, 125]. Extrinsic labels are mainly formed by near-infrared cyanine dyes which all consist of a similar molecular structure: a heterocyclic ring linked by a polymethine bridge. The fluorescent features are determined by the length of the bridge and the structure of the ring [108]. These extrinsic labels can be categorized as targeted or non-targeted. Targeted probes are divided into three groups which are defined by a unique intrinsic property or function of their respective target. The first group are simple targeting probes which are characterized by their attraction to a highly selective target. The connection between probe, for instance labeled antibodies, and target, such as specific cell surface receptors, is highly-affine and thus non-covalent [108]. The second group are cross-linking probes. They are smaller and lower affinity ligands and therefore have a higher specificity to their target. Chemical reactive groups were added to build up an irreversible covalent linkage [45, 97]. Enzym-activatable ‘smart’ probes are the last group of targeted probes and are only fluorescent after being catalysed by the target enzyme. Various diseases are attributable to the same molecular basis and thus ‘smart’ probes functioning as biomarkers could facilitate the early detection of diseases [93]. Examples of non-targeted dyes are indocyanine green (ICG) and fluorescein. ICG is an FDA-approved diagnostic drug for determination of blood volumes, cardiac output and hepatic function [44]. Fluorescein is an FDA-approved fluorescent dye applied in angiography. ICG and fluorescein can only

be used for cell labeling purposes, if assisted labeling techniques are applied. New non-targeted fluorochromes are designed continuously. Examples of these dyes are:

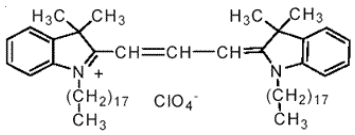

Fig. 2.4: DiI (1,1'-dioctadecyl-3,3,3',3'-tetramethylindocarbocyanine perchlorate), Molecular Probes, Invitrogen®

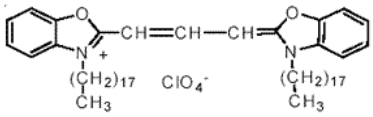

Fig. 2.5: DiO (3,3'-dioctadecyloxacarbocyanine perchlorate), Molecular Probes, Invitrogen®

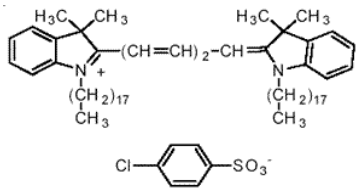

Fig.2.6: DiD (1,1'-dioctadecyl-3,3,3',3'-tetramethylindodicarbocyanine), Molecular Probes, Invitrogen®

This thesis is focused on the use of DiD as this dye demonstrates low cytotoxicity, high labeling efficiency in in vitro cell labeling and in vivo cell tracking with OI and high resistance to intracellular transfer. DiD and its analogues are lipophilic carbocyan markers and integrate into the cell membrane of the target cells after simple incubation by adding DiD to the cell suspension. It shows minor fluorescence as a free dye in water, but a marked fluorescence when incorporated into cells. The incubation time depends on the cell type and is between 5 and 20 minutes. The molecular weight is 1,052.08, and the excitation maximum is 644 nm, with an emission peak at 665 nm.

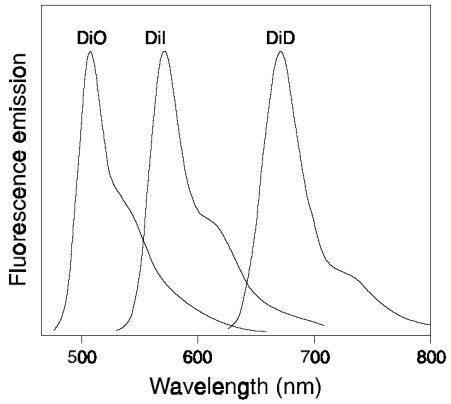

Fig. 2.7: Normalized fluorescence emission spectra of DiO, DiI and DiD bound membranes Molecular Probes, Invitrogen®

2.2.1.2 Labeling Techniques

Strategies for cell labeling include intrinsic and extrinsic labeling. Intrinsic labeling is defined as introduction of fluorescent genes into the promotor of other genes which consequently induces gene expression of these proteins [41]. Transfection is one method for in vitro labeling which describes the introduction of foreign material into eukaryotic cells using a virus vector. This vector contains the fluorescent gene. Examples for those vectors are retroviridae, herpesviridae and adenoviridae [37]. A recent development is the use of transgenic animals which contain multifunctional reporter genes e.g. GFP-luciferase fusion genes in mice [39]. Genetic abnormalities could be affected by insertion of a gene into the promoter. Thus the animals could experience malignancy, which is a risk for the validity of the cell tracking model [33]. The other strategy for the introduction of fluorescent dyes into cells is defined as extrinsic labeling. Extrinsic labeling is obtained through direct injection, simple incubation, electroporation or transfection. Direct injection techniques involve artificial incorporation into cells by using the technique of micropipettes, which is only feasible if a few cells are selected and the cells are fixed. Simple incubation labeling techniques involve incubating cells for a certain amount of time. As previously mentioned, endogenous labels can be classified into two groups, non-targeted and targeted dyes. Both can be labeled by simple incubation. For the non-targeted dyes the mechanism consists of adherence and diffusion of the lypophilic cyanine-based dye across the

phospholipid cell membrane bilayer. Further uptake mechanisms include transporters, endocytosis and phagocytosis. It is important to keep in mind that these mechanisms are enforced by using serum-free media. For the targeted dyes, such as DiD, the mechanism consists of the establishing a strong non-covalent or irreversible covalent bond whereby a catalytic reaction results in “dequenching” and effectively labels the cell target [9, 67, 112]. Electroporation involves applying an external electrical field and thus forming pores when the voltage across a plasma membrane exceeds its dielectric strength. During this period of time extracellular compounds can enter into the cell. Transfection is the introduction of DNA into eukaryotic cells using a virus vector or other means of transfer. Tracing of bi-functional labels is achieved by simple incubation and, in the majority of cases, is amplified by using Lipofectin and Lipofectamine [19].

2.2.2 Magnetic Resonance Imaging

2.2.2.1 Iron Oxides

A variety of iron oxides have been developed for contrast enhanced MRI. So far, two different types of iron oxides have been clinically approved or are in phase 3 trials: superparamagnetic iron oxides (SPIO) with a high R2/R1 relaxivity ratio and short blood half-life and ultrasmall paramagnetic iron oxides (USPIO) with a lower R2/R1 relaxivity ratio and longer blood half-life [85]. Contrast agents based on iron oxide are composed of an iron oxide core and a dextran, carboxydextran or starch coat, and function by creating local field inhomogeneities that cause a decreased signal on T2-weighted MR images [46, 114]. The most common iron oxide based cell-specific MR contrast agents are superparamagnetic iron oxide particles (SPIO) or ultrasmall SPIOs (USPIO). These SPIO and USPIO show a high sensitivity for depiction with MR imaging and a good, extensively investigated biocompatibility [46, 114, 116]. It was demonstrated through electron microscopy that USPIO particles transmigrate the capillary wall by means of vesicular transport and through interendothelial junctions [117]. The iron oxide particles are internalized into a large variety of cells which are either professional phagocytes such as macrophages in spleen, liver, lymph nodes, bone marrow or nonphagocytic cells such as tumor cells,

lymphocytes or neuronal cells. The two major pathways for the uptake mechanism are the Fc or C3b mediated phagocytosis in phagocytes for plasma opsonised iron oxides and fluid phase pinocytosis in nonphagocytic cells. Furthermore it was demonstrated that chemically modified dextran-coated iron oxides can be internalized through receptor-mediated endocytosis into highly specialized cells such as hepatocytes or pancreatic acinar cells [116]. The tumor-to-liver contrast is significantly increased in all iron oxides which allows the detection of more lesions than with unenhanced MRI on T2-weighted images. All iron oxides create a constant signal on T2-weighted accumulation phase images in malignant lesions without phagocytic cells. In benign lesions they generate a signal decrease with phagocytic cells or a significant blood pool on T2-weighted accumulation phase images. The signal decrease of benign lesions is useful for the lesion characterization as the signal decrease is proportional to the Kupffer cell activity or tumor vascularity. In addition the distinction between benign and malignant lesions is the ring enhancement of malignant lesions (metastases) on T1-weighted enhanced images either during the perfusion phase with Resovist or during the accumulation phase with Ferumoxtran [85].

2.2.2.2 Labeling Techniques

There are different alternatives for labeling various hematopoietic cells with SPIO and USPIO. The labeling can be achieved through simple incubation of the cells with the contrast agents ex vivo [19, 20, 66], or, more efficiently, by using transfection techniques with peptides [56], dendrimers [13], cationic liposomes [19, 20, 35] or protamine sulfate [4, 6]. As most lymphocyte populations do not spontaneously phagocytose contrast agents and are highly susceptible to potential toxic effects, lymphocytes are difficult to label with MR contrast agents [14, 18, 68, 91, 100, 126]. Only a few successful techniques for lymphocytes labeling with MR contrast agents have been reported [18, 24, 68, 100]. Tailored labeling techniques, which provide effective labeling in a short time period, are needed for these cells which have been developed by the aforementioned authors. In previous studies, efficient labeling techniques were established for lymphocytes and NK cells in particular, using second generation

SPIOs and various transfection techniques [18]. The intracellular presence of an iron-containing contrast agent is confirmed by Prussian blue staining of labeled cells. The iron oxide nanoparticle-based MR contrast agent is FDA-approved for MR imaging of liver diseases after intravenous injection. Ferumoxides are the most commonly used MR contrast agents for in vivo cell tracking with MR imaging in an experimental setting [4, 5, 18, 34, 66], and have been used for NK cell tracking in a clinical study in patients with melanoma [24]. Other SPIOs, such as ferocarbotran (Resovist; Schering AG, Berlin, Germany), which is approved for liver imaging in Europe, can also be utilized for labeling NK cells [18] and in vivo NK cell tracking.

2.3 In Vivo Cell Tracking

Molecular imaging techniques can help to detect cells and follow cellular processes non-invasively, using optical imaging, magnetic resonance (MR) imaging or nuclear imaging. New cell tracking techniques that provide a non-invasive in vivo detection of contrast agent labeled cells can directly verify or disprove accumulation of NK cells in the tumor tissue – a major requirement to assess the efficacy of adoptive immunotherapy. Labeling techniques with radioactive markers provide a high sensitivity but limited spatial resolution, and carry the risk of radiotoxic cell damage [2, 31, 65, 68]. As the techniques for tracking of NK cells have developed rapidly in recent years both qualitative and quantitative data can be provided.

2.3.1 Optical Imaging

2.3.1.1 OI Technique

Optical imaging is an imaging technique based on the detection of the light emitted by vital cells or tissue. There are two modes of optical imaging: fluorescence and biolumenescence. Fluorescence is dependent on fluorescent dyes or proteins which need to be excited by an external source of light. This source is a monochromatic laser which is tuned to the near-infrared spectra,

600-900 nm [123]. Fluorophores emit photons of that laser and therefore constitute an excited electronic state. Fluorescence occurs when the molecules relax to their ground state after being excited for a specified amount of time. Biolumenescence imaging needs no excitation by an external source and in comparison to fluorescent imaging provides lower significant background noises created by autofluorescence of endogenous molecules. The use of fluorescent imaging red proteins is preferred because their wavelength is above the hemoglobin spectrum [86]. A limitation of the technique is that a major portion of light is lost due to absorption and scattering (10-fold per cm tissue). As fluorescent signals are more intense when the labeled cells are located in the surroundings of the surface, they are best used for small animals or superficial pathological processes [59]. Transmission of light is highest in skin and muscle cells and lowest in vascularized tissues. High near infrared spectra are advantageous for depiction of fluorescent dyes in all tissues, because the depth of penetration is higher and the autofluorescence is lower in comparison to near-infrared dyes like GFP. Photons that have been emitted from a bioluminescent or fluorescent probe are received by the Charge Coupled Device Camera (CCD) which is a pixelated silicon detector. Using this method photons are changed into pixels and recorded by a remote computer. In order to minimize background noise the CCD Camera has to be cooled down. Subsequently a filter is used to allow only the fluorescence signal of the chosen probe to reach and be detected by the CCD camera. During an OI study the following items have to be kept constant: laser voltage, filters, exposure time, binning and the field of view [127]. Standard images are composed of two images: one photographic and one fluorescent. The fluorescent picture can be used alone or can be combined with the corresponding photograph or “bright light” picture. There are some limitations of OI including the dependence of depth penetration, light absorption and scattering of tissue and the 2D representation. However, OI also has many advantages over other imaging techniques including rapidness, no irradiation exposure and molecular sensitivity. Furthermore it is nontoxic, reproducible and inexpensive [125].

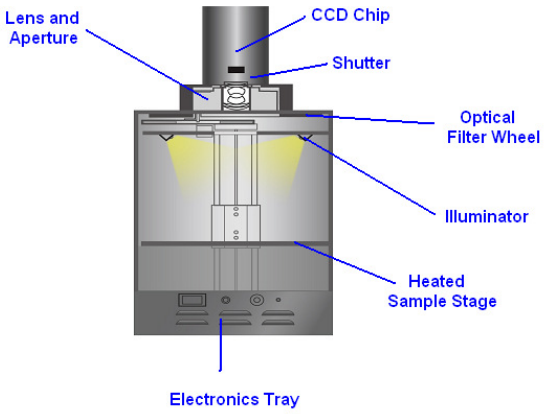

Fig. 2.8: Xenogen's IVIS 50 Imaging system utilizing fluorescence reflectance imaging[36]

2.3.1.2 Cell Tracking with OI

The obvious merit in evaluating molecular level sensitivity in optical imaging is comparable to that of conventional nuclear imaging and is significantly higher than the resolution acquired with MRI. Rapid image acquisitions (<5 min) are provided with close follow-up studies of the in vivo kinetics of labeled NK cells. It is possible to assess whole animals in experimental implementation [101]. The NK cells are injected locally or systemically to determine their in vivo kinetics, to assess dynamic changes in NK cell tumor accumulation over a specific period of time and to evaluate the time point of maximal NK cell tumor accumulation. In order to get more detailed anatomical information the technique is changed from optical imaging to MR Imaging once this maximum of tumor accumulation has been achieved by the optical imaging technique. Therefore this inexpensive and fast method can reliably analyze both the presence or absence of NK-cell accumulation in prostate cancers as well as the time point of maximal NK cell tumor accumulation.

2.3.2 Magnetic Resonance Imaging

2.3.2.1 MRI Technique

MR imaging provides several advantages for the tracking of NK-cell immunotherapy including 3D information, high anatomical resolution, well-

defined soft tissue contrast and no irradiation to the cells or the patient. Disadvantages of MR compared to optical or radiotracer based imaging techniques are limited sensitivity and expensive equipment, which limits close follow up studies. A large number of variable parameters affect the sensitivity of the MR technique, such as field strength, pulse sequence parameters and the nature of coils being utilized. Extensive training and knowledge is needed to fully utilize the advantages of this technique. Nevertheless, MR imaging is one of the most attractive imaging modalities with regard to its potential for translational applications. While approved for other applications, the required MR contrast agents are not yet FDA-approved for cell labeling and in vivo cell tracking techniques and are therefore used off-label. Initial MR-based NK-cell tracking studies in patients have already been performed [24].

2.3.2.2 Cell Tracking with MRI

MR imaging has the distinct advantages of providing three-dimensional data with high anatomical resolution (< 1 mm in plane), a high soft tissue contrast, and is not associated with any irradiation exposure [5, 6, 13, 20, 35, 43, 66, 116]. The accumulation of NK cells in the tumor can be proved or refuted by MR imaging at near microscopic anatomical resolution. The subject is therefore not exposed to any radiation and tracking the cells is accomplished non-invasively. A great advantage of MR towards optical imaging is the detection of the delivery of NK cell immunotherapy to deep-seated target tissues. This is inaccessible to optical imaging. At 30 minutes after injecting the labeled cells are well visualized locally close to the tumor at the site of injection. This observation at an early stage in the imaging process is an important means to confirm the successful delivery of the labeled cells. It has been observed consistently that the labeled cells accumulate around the periphery of the tumor 24 hours after injection. The first explanation for this phenomenon is that there is more vascularity in the periphery of the tumors and the NK cells migrate to that location. The second explanation is that the intratumoral pressure is higher than the surrounding pressure. Hence the cells move to the subcutaneous tissue where the pressure is lower. In general the intratumoral pressure is very high because of high interstitial pressure [57, 83]. Although the tumor is centrally necrotic, NK cells

can also migrate to the necrotic tissue when they are injected intratumorally. In this case the labeled cells stay in the necrosis and do not move to the periphery. It has to be considered that the NK cells may die in this tissue as they do not get any oxygen or nutrients and this will consequently lead to failure of treatment. To circumvent this problem of intratumoral injection imaging-guided cell injections or other routes of NK-cell delivery, such as arterial or systemic venous cell administration, are used. De Vries et al. conducted a clinical study where they effectively tracked dendritic cells in vivo after intranodal injection of magnetically labeled cells. It was possible to detect very low numbers of dendritic cells in the MR imaging in humans and to receive detailed anatomical information. The major advantage of MRI over scintigraphy is that accuracy of dendritic cell delivery and of inter- and intra-nodal cell migration patterns can be assessed. All in all it was shown that MR cell tracking using iron oxides appears to be clinically safe and well suited to monitor cellular therapy in humans [24].

2.3.3 Combination of OI and MRI

A combination of optical and MR-based cell tracking techniques is advantageous for certain applications, as it is possible to benefit from both techniques: optical imaging offers high sensitivity and frequent observations while MR imaging contributes high resolution and improved depth of penetration. Few contrast agents, for instance gadolinium-rhodamine nanoparticles, gadophrin-2 and gadofluorine-Cy-3 can be detected both by MR as well as optical imaging. Another possibility to achieve a combination of optical and MR imaging is double labeling: the cells are first labeled by ferumoxides using the standard protocols and subsequently labeled by fluorochromes such as DiD. In this way optimal intracellular concentrations can be achieved for both modalities and a visualization on both is possible [19, 34, 101].

3 Material and Methods

3.1 Cell Lines

3.1.1 Prostate Cancer Cell Lines DU-145, PC-3 and LNCaP

As prostate cancer is the second leading cause of cancer-death for men in western countries, progress made in this field of research is in the interest of the scientific community. There are several prostate cancer cell lines which are used for research. The three most common are DU-145, PC-3 and LNCaP and are thus chosen for this thesis. The DU-145 and PC-3 cell lines were both developed from human prostatic adenocarcinoma, DU-145 from brain and PC-3 from bone metastasis. LNCaP was also developed from a human prostatic adenocarcinoma, but from a lymph node metastatic lesion [3]. All three cell lines have the potential to metastasize. However, the cell lines have different levels of gradation starting with PC-3 with the highest potential, DU-145 with a moderate level and LNCaP with the lowest potential. As a result PC-3 cells are 14-fold more invasive and DU-145 9-fold more invasive than LNCaP. The invasion of cancer cells through the extracellular matrix is often associated with a high level of expression of one or more proteases. Pulukuri et al. showed that an augmented expression of the protease urokinase plasminogen activator (uPA) and its receptor (uPAR) lead to an increased invasiveness [81]. All three cell lines express the protein of an androgen receptor which is a phosphoprotein like other steroid hormone receptors. It can be activated or stabilized by its phosphorylation. The mRNA of the receptor could be detected in all three cell lines, but with very different levels of intensity. DU-145 and PC-3 express the protein in much lower amounts as levels of androgen receptor mRNA in DU-145 were about 50% lower than in LNCaP and even lower in PC-3. Since the

androgen receptor up-regulates the expression of p21 protein, which is an inhibitor of cyclin-dependent kinases, the protein is down-regulated in PC-3. The fact that the protein can be up-regulated by DHT treatment is evidenced as DU-145 and PC-3 express detectable levels of AR mRNA. DU-145 and PC-3 are considered AR-positive cell lines. However, as the AR protein is indeed up-regulated when treated with DHT, the activity of the AR-positive reporter gene is not stimulated, therefore DU-145 and PC-3 are considered to be androgen non-responsive [3, 61]. LNCaP cells in contrast to these two prostate cancer cells are androgen-responsive. Kokontis et al. have created LNCaP sublines which are androgen-independent. These cells emerged out of common LNCaP cells by denial of androgens. Although the cells are androgen-independent they express the androgen receptor with a higher level and also express prostate specific antigen when treated with androgens. Unlike the common LNCaP, the sublines are inhibited by androgens [50, 111]. In addition DU-145 together with PC-3 does not express PSA, contrary to LNCaP which produces a considerable amount [72, 98]. Ligeza et al. showed that DU-145 produces a significant quantity of the growth factor VEGF which is regulated by three different autocrine loops: IGFII/IGFIR, VEGF/VEGFR2 and TGFα/EGFR. This fact may explain why it is so difficult to find specific tyrosine kinase inhibitors in the therapy of prostate cancer [60]. All three prostate cancer cell lines used in this thesis were grown in RPMI 1640^{+++} medium (Bio Whittaker) supplemented with 10% heat-inactivated FBS, 2 mM L-glutamine, 100 units/mL penicillin, and 100 µg/mL streptomycin. As the prostate cancer cell lines all are adherent they need to be trypsinized for culturing. Therefore the culture medium has to be removed and discarded. Then the cell layer has to be rinsed briefly with 2 mL of Trypsin-EDTA solution as this step removes the trypsin inhibitor. After this, the flask is placed in an incubator (Binder, IBS Integra) at 37°C for 5 minutes. During that period it is important not to shake the flask as this may cause clumping. Next the flask is put under a microscope and the cells are observed to find out if they are already dispersed. If not they are put into the incubator again for another 5 minutes. 6 to 8 mL of RPMI 1640^{+++} are added and the cells are aspirated by gentle pipetting. Depending on how many cells are required, a suitable number

of cells is put in new flasks for culturing and are incubated at 37°C without CO_2. The medium for culturing the cells is ideally changed 2 to 3 times a week.

3.1.2 Breast Cancer Cell Lines MCF-7, MDA-MB-453

Breast cancer is the leading cancer affecting women in western countries. The two breast cell lines used in this thesis are MCF-7 and MDA-MB-453. MCF-7 was first established by Soule et al. in 1973 and is named after their institute in Detroit Michigan Cancer Foundation. Before this it was only possible to culture breast cancer cell lines which lived for a few months. MCF-7 cells date back to a pleural effusion which was taken by a patient suffering from metastatic breast cancer. The primary tumor was an invasive breast ductal carcinoma. It is described that estrogen receptors exist on MCF-7 cells and that the cells can be stimulated by and respond to estrogen. In addition estrogen is able to reverse the inhibition of MCF-7 cells if the cells are inhibited by tamoxifen, an antagonist of the estrogen receptor in breast tissue. Estrogen receptors as well as progesterone receptors are synthesized on the cells. These receptors are intracellular steroids that specifically bind progesterone [55]. Lacroix et al. described that ER-positive, low-grade and well-differentiated breast tumours are mostly luminal epithelial phenotypes, as is MCF-7. The other tumours, that are ER-negative, high-grade and poorly differentiated breast tumors, are at the most basal myoepithelial phenotypes. Of all eight cell lines which were tested in the NCI study (MCF-7, MCF-7/Adr, MDA-MB-231, Hs578T, MDA-MB-435, MDA-N, BT-549 and T-47D) MCF-7 was the only cell line in which there was no mutation present in p53, a tumor suppressor protein in humans. Also MCF-7 was the most sensitive cell line of all. After treating MCF-7 which normally express ERBB2 with AKT (protein kinase B), a serine/threonine protein kinase that is involved in the glucose metabolism, apoptosis, cell proliferation, cell migration and transcription the cells were more resistant against apoptosis. MCF-7 expresses low levels of mRNA for FGFRs which are receptors that bind to ligands of the fibroblast growth factor family of proteins [52]. MDA-MB-453 is a human breast carcinoma cell line established from an effusion of a 48-year-old woman with breast carcinoma in 1976 [12]. This breast cancer cell line

responds to VEGF, expresses high levels of mRNA of FGFR (fibroblast growth factor receptor) and has elevated levels of FGF receptors. To be precise MDA-MB-453 expresses a relatively small amount of FGFR 1, FGFR 2 and FGFR 3, but a relatively large amount of FGFR 4. Another growth factor ERBB2 (human epidermal growth factor receptor 2) is also expressed by MDA-MB-453 [64]. Similar to MCF-7 this cancer cell line belongs to the luminal epithelial phenotypes. Other than MCF-7 this cancer cell line expresses high levels of androgen receptors [122] but is estrogen-receptor-negative and progesterone-receptor-negative [26]. MCF-7 cells and MDA-MB-453 cells were maintained in Dulbecco modified Eagle medium ($DMEM^{+++}$; Bio Whittaker, Verviers, Belgium) containing 10% heat-inactivated fetal bovine serum (FBS), 2 mM L-glutamine, 100 units/mL penicillin, and 100 ⌟ g/mL streptomycin. Since both breast cancer cell lines are adherent they are trypsinized, as is the case with prostate cancer cell lines. Therefore the culture medium has to be removed and discarded. In the next step the cell layer has to be rinsed briefly with 2 mL of Trypsin-EDTA solution as this step removes the trypsin inhibitor. The flask is placed in an incubator (Binder, IBS Integra) at 37°C for 5 minutes. Once again it is important not to shake the flask as this may cause clumping. Next the flask is put under a microscope and the cells are observed to see if they are already dispersed. If not they are put back into the incubator for another 5 minutes. 6 to 8 mL of $DMEM^{+++}$ are added and the cells are aspirated by gentle pipetting. Depending on how many cells are required a suitable number of cells is put in new flasks for culturing and the cells are incubated at 37°C without CO_2. The medium for culturing the cells is ideally changed 2 to 3 times a week.

3.1.3 Reference Cell Line K562

The reference cell line K562 was established in 1975 by Lozzio et al. from the pleural effusion of a 53-year-old female who suffered from chronic myelogenous leukemia and it is the first human continuously growing leukemia cell line. K562 cells display the Philadelphia Chromosome even after the cells are cultured for a long time. Three facts show that the K562 cell line is not another lymphoblastoid cell line. First of all the EBV and herpes-like viruses which are

present in lymphoblastoid cells are lacking. In addition the K562 cells are unable to produce immunoglobulins which is proven in lymphoblastoid cells [62]. In contrast to the prostate and breast cancer cell lines K562 cells are suspension cells which means they are non-adherent [16]. K562 are erythroid precedent cells in a very early stage so that they do not express any antigens [49]. As the major histocompatibility complex (MHC) is absent in K562 cells they are not able to restrain the NK activity and are easily killed by NK cells. As a result they are very useful for NK cell assays. K562 cells are positive for the bcr-abl fusion protein [17]. Human erythroleukemic K562 cells were grown in medium (Bio Whittaker) supplemented with 10% heat-inactivated FBS, 2 mM L-glutamine, 100 units/mL penicillin, and 100 µg/mL streptomycin. The NK cells are suspension cells, which means that they are not trypsinized for culturing. Depending on how many cells are required, an appropriate number of cells is placed in new flasks for culturing. 6 to 8 mL RPMI 1640^{+++} is added and the cells are incubated at 37°C without CO_2. A recommended ratio is 1:2 to 1:6. The medium for culturing the cells is ideally changed 2 to 3 times a week.

3.1.4 NK Cell Lines NK-92, NK-92-scFv(FRP5)-ζ, NK-92-scFv(MOC31)-ζ and NK-92-scFv(FRP5)-mζ

The characteristics of the parental NK cells are described above in 2.1.2. The high cytotoxic activity of these cells mediated by perforin and granzym was amplified by establishing genetically modified NK-92 cells. These cells express chimeric antigen receptors that are specific to the tumor-associated EpCAM antigen or for the tumor-associated ErbB2 (HER2/neu) antigen. EpCAM stands for ‘Epithelial Cell Adhesion Molecule’ and is a member of the cell adhesion receptors (CAMs). CAMs are actively involved in regulating various cell processes such as growth, differentiation and cell death. EpCAM protein overexpression emerges in many human tumors of epithelial origin [119]. EpCAM is a type I transmembrane glycoprotein and consists of an extracellular domain containing two epidermal growth factor (EGF)-like repeats, and a short intracellular domain of 26 amino acids in which two binding sites for alpha-actinin are present for linkage to the actin cytoskeleton. It is expressed at the

basolateral membrane of cells [10]. ErbB2 (HER2/neu) signifies 'human epidermal growth factor receptor 2' and is a member of the EGF-receptor-related family of receptor tyrosine kinases. It is cell membrane surface-bound and is a factor in signal transduction pathways leading to cell growth and differentiation. In many human tumors of epithelial origin c-erbB2 gene amplification and ErbB2 protein overexpression have been observed. A connection to cancer development and progression has been made [73, 110].

The genetically modified NK-92 cells which improve the antitumoral activity of parental NK-92 cells are generated by transduction with a retroviral vector encoding a chimeric antigen receptor. The receptor was produced by fusion of the specific single-chain (sc) Fv antibody fragments to the signal transducing CD3 zeta chain of the T-cell receptor and a flexible hinge region derived from CD8 [109]. In this thesis three different genetically modified NK-cell lines were used. Firstly the NK-92-scFv(FRP5)-ζ cell line, which is created by fusion with the antibody fragment scFv(FRP5) that is ErbB2 specific. Secondly, the NK-92-scFv(FRP5)-mζ cell line, which is also created by fusion with the antibody fragment scFv(FRP5) and finally the NK-92-scFv(MOC31)-ζ cell line, which is created by fusion with the antibody fragment scFv(MOC31) that is EpCAM specific. All transduced NK cell lines express high levels of the fusion proteins on the cell surface and these can be detected by FACS analysis [119]. Human NK-92 cells were propagated in X-Vivo 10** and the transduced NK-92-scFv(FRP5)-ζ, NK-92-scFv(MOC31)-ζ and NK-92-scFv(FRP5)-mζ cells were propagated in X-Vivo 10*** medium (Bio Whittaker) supplemented with 5% heat-inactivated human serum, 100 units/mL IL-2 (Proleukin, Chiron, Emeryville, CA), and 0.6 mg/mL G418 (NK-92-scFv(FRP5)-ζ / NK-92-scFv(MOC31)-ζ / NK-92-scFv(FRP5)-mζ). The NK cells are suspension cells: they are not trypsinized for culturing. Depending on how many cells are required, an appropriate number of cells is placed in new flasks for culturing, 6 to 8 mL X-VIVO 10 medium is added and the cells are incubated at 37°C without CO_2. The medium for culturing the cells is ideally changed 2 to 3 times a week.

3.2 Cell Labeling

3.2.1 Optical Imaging

3.2.1.1 DiD

In this thesis DiD ($C_{67}H_{103}ClN_2O_3S$; 1,1'-dioctadecyl-3,3,3',3'-Tetramethyl-indodicarbo-cyanine, Vibrant cell labeling solution, Molecular Probes, Oregon, USA) was used as this dye demonstrates low cytotoxicity, high labeling efficiency in vitro cell labeling and in vivo cell tracking with OI and high resistance to intracellular transfer. DiD integrates into the cell membrane of the target cells after simple incubation by adding to the cell suspension. It is a non-targeted, lipophilic, carbocyanine near-infrared (NIR) fluorochrome with a molecular weight of 1052.08DA and an excitation maximum of 644 nm, with an emission peak at 665 nm.

3.2.1.2 Labeling Techniques

For labeling the NK cells with DiD they are counted at first. The culture media is removed and the cells are washed once with phosphate-buffered saline (PBS) or serum-free media. The cells are re-suspended at a density of around 1 million cells per mL of serum free media. Prior to labeling, the cell viability is measured via Trypan Blue Test. Then 5 µl of DiD per mL of cell suspension is added, mixed well by gentle pipetting and the suspension is incubated at 37°C for 15 minutes. The cell viability is then measured again. The labeled suspension tubes are centrifuged (5min, 400rcf, 25°C), the supernatant is removed and the cells are gently re-suspended in PBS (pH 7.4). The wash is repeated twice more in order to wash off the remaining DiD that had not been incorporated into the cell membrane.

3.2.2 Magnetic Resonance Imaging

3.2.2.1 Endorem

The ferumoxide Endorem was used for labeling NK cells in this thesis. Ferumoxides (Endorem; Lab. Guerbet, Aulnay-sous-Bois, France and Ferridex; Berlex Laboratories, USA) are superparamagnetic iron-oxide particles (SPIO) with a high R2/R1 relaxivity ratio of 160/40, a diameter of 120–180 nm (mean 150 nm) and a short blood half-life (minutes). After injection most of the particles accumulate in the liver, the rest in the spleen within minutes after administration. The maximum of liver signal intensity is reached ½ hour to 6 hours after administration and returns to normal within 7 days [115]. They are colloid-based and consist of nonstoichiometric magnetite cores. These are covered with a dextran T-10 layer. In dissolved condition they consist of polycrystalline aggregates [46, 114].

3.2.2.2 Labeling Techniques

For labeling the NK cells with Endorem they are counted at first. Around 10 mio cells are plated into a T225 flask. Next the culture media is taken off and the cells are washed once with PBS or serum-free media. They are resuspended at a density of around 1 million cells per mL of serum free media. Prior to labeling, the cell viability is measured via Trypan Blue Test. Then 100 µl of ferumoxide per mL of cell suspension is added and the suspension is incubated at 37°C for 12 hours. After this the cell viability is measured again. The cells are washed three times with PBS in order to wash off the remaining iron that was not incorporated into the cells. In order to internalize the iron better into the cells the labeling media has to be prepared with protamin sulfate. Therefore 100 µl of ferumoxide per mL of cell suspension are mixed in 2 mL serum free media and 5 µl Protamin. The solution is left to stand for 10 min at 37°C. All other steps are the same as previously described. Another approach used in this thesis is to prepare the labeling media with lipofectin. The used amount of ferumoxide is mixed in 2 mL serum free media and the equal amount of lipofectin is also mixed in 2 mL of serum free media. These two solutions are left to stand separately for 30 min at 37°C. After this the solutions are mixed and are left to

stand for another 30 min at 37°C. All other steps are equal to the aforementioned.

3.3 In Vitro Studies

3.3.1 Trypan Blue Test

The Trypan Blue Test is used to determine the viability of cells in a cell suspension. The suspension is mixed with the dye, in this case trypan blue, in others eosin or propidium. The dye is either excluded or incorporated depending on whether the cell membrane is intact or not. Under the microscope, the cells that can be distinguished as living have a clear cytoplasm, which would appear blue in the event the cells were dead. Hereafter the steps of the protocol for the Trypan Blue Test are described. First of all a small amount of the cell suspension is centrifuged and the supernatant is discarded. Thereby the number of cells has to be a suitable amount to be counted in the hemacytometer. The cell pellet is resuspended in 1 mL serum-free complete medium, as serum proteins stained with Trypan Blue could produce deceptive results. Next one part of 0.4% Trypan Blue and one part of the prepared cell suspension are mixed so that 10 to 20 µl of each part is put into a small plastic tube. The composite is incubated for three minutes at room temperature. If the incubation time lasts longer than three to five minutes, it will lead to a reduced viability of the cells as Trypan Blue causes cell death. A drop of the composite is placed in a hemacytometer and viewed through a binocular microscope. The next step is to count the viable and the nonviable cells, i.e. the unstained and stained cells. The total number of viable cells per mL is calculated by multiplying the total number of viable cells by 2. The total number of cells per mL is calculated by adding up the total number of viable and nonviable cells and multiplying by 2.

3.3.2 Prussian Blue Test

Intracellular presence of iron-containing contrast agent was confirmed by Prussian blue staining of labeled cells. In order to get the NK cells onto the glass slices a special slice centrifuge (CellSpinII, Tharmac) was used. After letting the centrifuge run with 200 µl of PBS, 1 x 10^6 cells were resuspended in 250 µl PBS and centrifuged onto the glass slices. These were dried over night. The next day the slices were put into iron reagent, a mixture of two components of 2% kaliumhexacyanoferrat II (dissolve in distilled water) and one component of 1 % HCl for 20 min. The slices were then washed in distilled water for 15 sec. For counterstain nuclear fast red solution was used for 8 min. After washing the slices in distilled water for 30 sec they were dehydrated and covered by a cover slip. The Prussian Blue Test was arranged for parental NK-92 cells, NK-92-scFv(FRP5)-ζ, NK-92-scFv(MOC31)-ζ and NK-92-scFv(FRP5)-mζ cells. For every cell line samples of labeled cells with Prussian blue test were provided, as were samples of unlabeled cells with Prussian blue test as control and samples of unlabeled cells with just nuclear fast red. Images were captured with a special digital microscope camera (Axiocam CCD Kamera, Zeiss). Every picture was taken in 10 times and 20 times magnification.

3.3.3 Analysis of Chimeric Antigen Receptor Expression

The chimeric antigen receptor scFv(MOC31)-ζ, scFv(FRP5)-ζ or scFv(FRP5)-**m**ζ are expressed on the cell-surfaces of the different NK cells. This was determined by fluorescence activated cell sorter (FACS) analysis. The myc-tag specific monoclonal antibody (mAb) 9E10 was incubated with single cell suspensions of 5x10^5 Endorem labeled or non-labeled NK-92, NK-92-scFv(MOC31)-ζ, NK-92-scFv(FRP5)-ζ or NK-92-scFv(FRP5)-mζ cells for 1 hour at 4°C. After this, the cells were washed twice with PBS and incubated for another 30 min at 4°C with PE-labeled goat anti-mouse IgG secondary antibody (Dianova, Hamburg, Germany). For the analysis of the fluorescence of the cells a FACScan (Becton Dickinson, Heidelberg, Germany) was used.

3.3.4 Cytotoxicity Assays

This assay was conducted to determine the cytotoxicity of parental and genetically modified NK92 cells. The target cells (DU145, PC-3, LnCAP, MCF-7, MDA-MB-453 and K562) were incubated for 5 minutes at room temperature with the fluorescent dye carboxyfluorescein succinimidyl ester (CFSE) (Sigma, Deisenhofen, Germany) in order to differentiate them from the effector cells. After two washing steps with 15 mL of phosphate buffered saline (PBS) the labeled cells ($5x10^4$ in 100 µL growth medium/tube) were seeded in polypropylene tubes before the addition of 100 µL/tube of medium to determine spontaneous lysis or 100 µL of NK-92, NK-92-scFv(MOC31)-ζ, NK-92-scFv(FRP5)-ζ or NK-92-scFv(FRP5)-mζ cells at various effector to target ratios (E/T) of 1:1, 5:1, 10:1. Following 2 hours of incubation at 37°C, the cells were centrifuged for 5 min at 500 x g, the supernatant was removed and 200 µL/tube of a propidium iodide solution, a red DNA-dye for distinguishing dead cells from living ones (1 µg/mL in PBS), was added. Double positive cells (green and red) presented the dead target cells. After incubation for 5 to 10 min at room temperature, fluorescence was determined using a FACScan. Specific cytotoxicity was calculated using CellQuestPro software (BD Biosciences, Bedford, MA). Finally the number of double positive cells was determined, i.e. the dead target cells as they were quantified as CFSE and PI positive. The number of spontaneously lysed target cells was substracted to determine the specific lysed target cells with the appropriate standard deviation (Becton Dickinson, Heidelberg, Germany).

3.4 In Vivo Studies

3.4.1 Animal Model

The in vivo study was approved by the animal care and use-committee at the UCSF and was conducted in twelve male athymic rats which were six to eight weeks old. The animals were anesthetized with isoflurane for the tumor implantation, the OI scans and the NK cell injections. The prostate cancer cell

line DU-145 was used for the implantation. An amount of $5x10^6$ of the prostate cancer cells was injected subcutaneously next to the liver of all twelve animals. For this purpose the cells were mixed with 250 µl PBS and 250 µl Matrigel and were injected with a 26-gauge needle. The tumor size was measured every day until the average diameter reached 1.2 cm. After that the rats were divided into two equal groups. The first six rats received injections of parental NK-92 cells labeled with DiD into their tail vein. The genetically modified NK-92-scFv(MOC31)-ζ cells likewise labeled with DiD were injected into the tail vein of the other six rats. Before and after every NK cell injection the rats underwent an optical imaging scan.

3.4.2 Optical Imaging Protocol

The IVIS 50 small animal imaging system (Xenogen, Alameda, CA) and the Cy5.5 filter set (excitation: 615-665nm and emission: 695-770nm passbands) were used for the in vivo optical imaging studies. Seven days before the imaging started the rats received non-fluorescent food. The rats were anesthetized with isoflurane for the OI imaging. They were put into the light-tight heated imaging chamber at 37°C and pictures of two positions were taken: one of the anterior abdomen and the other of the left lateral abdomen. For each adjustment equivalent illumination parameters (exposure time=2 seconds, lamp level=high, filters=Cy5.5 and Cy5.5bkg, f/stop=2, field of view=12cm, binning=4) were chosen. Gray scale reference photographic images were conducted under low-level illumination. Optical Imaging scans were obtained before and at 1.5 hours, 8 hours and 24 hours post injection of the parental NK-92 or the genetically modified NK-92-scFv(MOC31)-ζ cells. After the last scan the rats were sacrificed by injecting them an overdose of Pentobarbital. To analyse the tumor and the organs (liver, spleen, lungs, bone) more closely, they were removed and placed into the OI chamber for an ex vivo scan. The parameters remained the same as for the in vivo scans. The tumors were also retained and used for fluorescence microscopy.

3.4.3 Fluorescence Microscopy

Fluorescence microscopy was performed with all the prostate tumors. For this purpose they were removed from the sacrificed rats after the last OI scan which was conducted 24 hours after the NK-cell injection and stored in tissue freezing medium at -80°C. The NK cells were detected by the NK cell specific CD 94 immunostaining wherefore 5 µm thick slides of the tumors were established. A Zeiss LSM510 confocal microscopy system equipped with krypton-argon and UV lasers was used to visualize the DiD dye (Red/Cy5 channel), FITC (green channel) and DAPI (blue channel). DAPI which is contained in mounting medium was applied for mounting the tumor nuclei. The images were acquired using LSM version 5 software.

3.4.4 Data Analysis

The Living Image 2.5 software was used to analyse the OI images. The software creates two different images: one photographic and one fluorescent image, which are superimposed. In order to standardize the optical imaging the images were measured in units of average efficiency, compared to a reference image and rectified for background signal. For the analysis of in vivo images regions-of-interest (ROI) were specified by surrounding the tumor.

3.4.5 Statistics

The statistical analysis was performed by the statistical department at the UCSF. Data were presented as means +/- standard deviations of each independent measurement. Statistical significance was assigned for p-values <0.05. The student's t-test was used to analyse the results for significant differences. Power calculations resulted in a minimal number of six animals in each experimental group. A two-way analysis of variance for comparisons of experimental groups that received genetically modified or parental NK cells was assumed with a significance level of 0.05 and will have 91% power to detect a variance among the two NK cell lines by means of 25% of a standard deviation. The analysis will have 97% power to detect a variance among the presence or

absence of NK cells in the tumor tissue by means of 25% of a standard deviation, assuming that the common standard deviation is 1.000 at a sample size of six. Differences of more than 1.5 of the standard deviation will be detected by 80% power. The assumed differences are far less than the expected differences.

4 Results

4.1 In Vitro Studies

4.1.1 Trypan Blue Test

In the in vitro experiments the cell viability was evaluated by means of the Trypan Blue Test. Therefore the cells were tested before and after any treatment. Especially after labeling the cells it was important to check the viability. At first the cells were labeled for 20 hours; however, subsequently over 40% of the cells died. For that reason the labeling time was reduced to 12 hours and as a result the percentage of dead cells was decreased to 15 %.

4.1.2 Prussian Blue Test

The Prussian Blue Test was arranged for parental NK-92 cells, NK-92-scFv(FRP5)-ζ, NK-92-scFv(MOC31)-ζ and NK-92-scFv(FRP5)-mζ cells. For every cell line Prussian Blue stains of labeled cells, Prussian Blue stains of unlabeled cells as control and stains of unlabeled cells with just nuclear fast red were provided. Every stain was photographed in both 10 and 20 times magnification and in each case the best image was chosen. Labeled NK 92 cells stained bright blue confirmed the intracellular presence of iron as well as the adequacy of labeling. Non labeled NK cells exposed to Prussian Blue do not show any blue staining suggestive of iron.

NK-92 cells

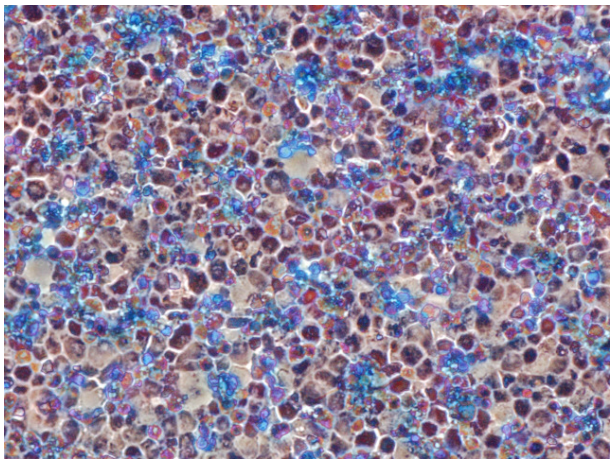

Fig. 4.1: NK-92 cells were fixed and labeled with Prussian Blue stain. The cells stained bright blue confirm the intracellular presence of iron as well as the adequacy of labeling.

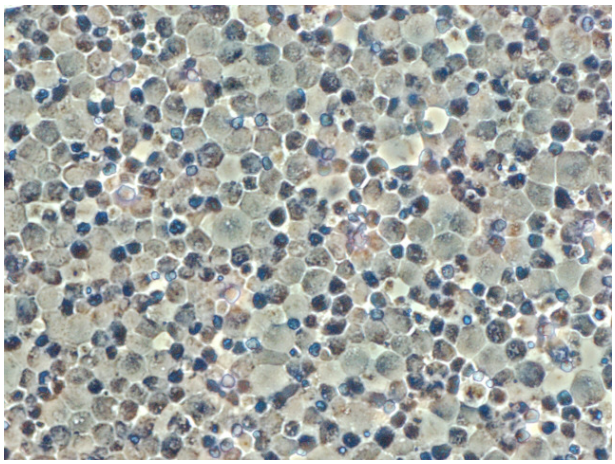

Fig. 4.2: Unlabeled NK-92 cells exposed to Prussian Blue do not show any blue staining suggestive of iron.

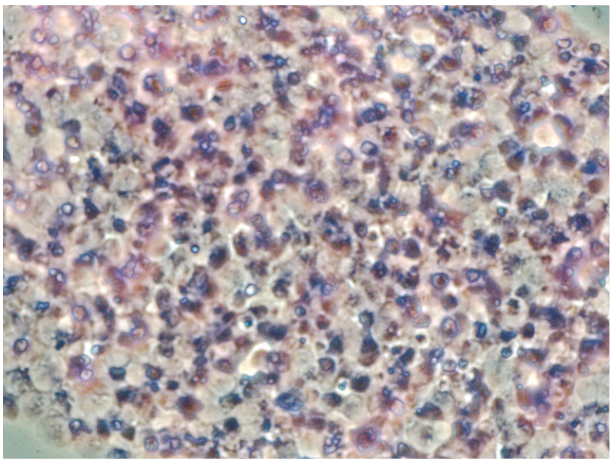

Fig. 4.3: Unlabeled NK-92 cells with nuclear fast red counterstain.

NK-92-scFv(MOC31)-ζ cells

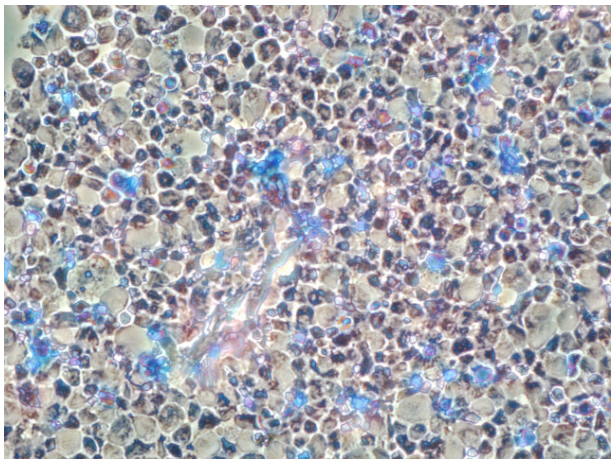

Fig. 4.4: Similar to NK-92 cells, NK-92-scFv(MOC31)-ζ cells were fixed and labeled with Prussian Blue stain. The occurrence of iron is verified by the blue inking of the cells. The capacity of labeling is verified with this.

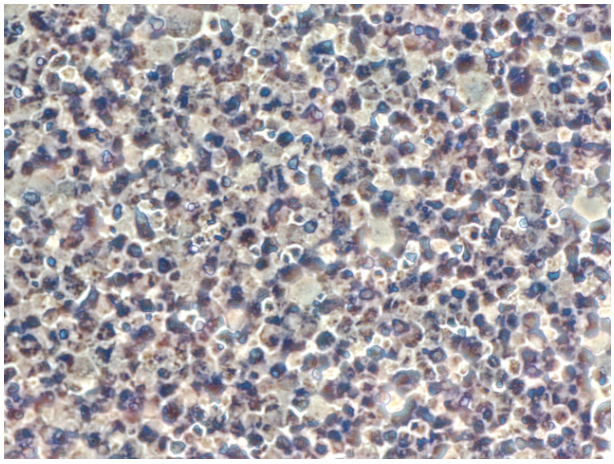

Fig. 4.5: Unlabeled NK-92-scFv(MOC31)-ζ cells stained with Prussian Blue. The lack of blue staining demonstrates the absence of iron and the validity of the Prussian Blue Test.

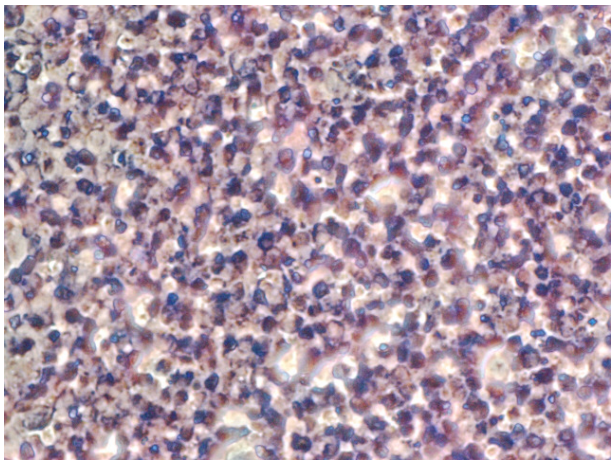

Fig. 4.6: Unlabeled NK-92-scFv(MOC31)-ζ cells with nuclear fast red counterstain.

NK-92-scFv(FRP5)-ζ cells

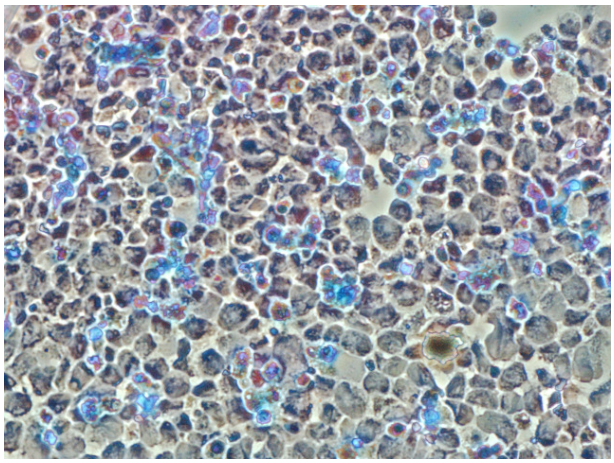

Fig. 4.7: NK-92-scFv(FRP5)-ζ cells were fixed and labeled with Prussian Blue stain. The blue dyed cells demonstrate the intracellular presence of iron. Hereby the adequacy of labeling is also confirmed.

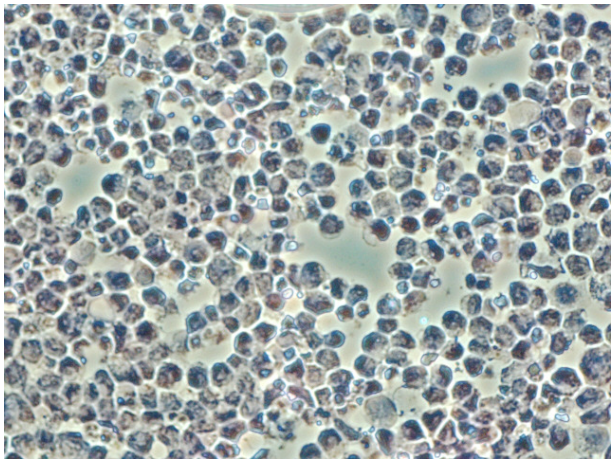

Fig. 4.8: Unlabeled NK-92-scFv(FRP5)-ζ cells do not show blue staining as an indication of intracellular iron although they were exposed to the Prussian Blue Test.

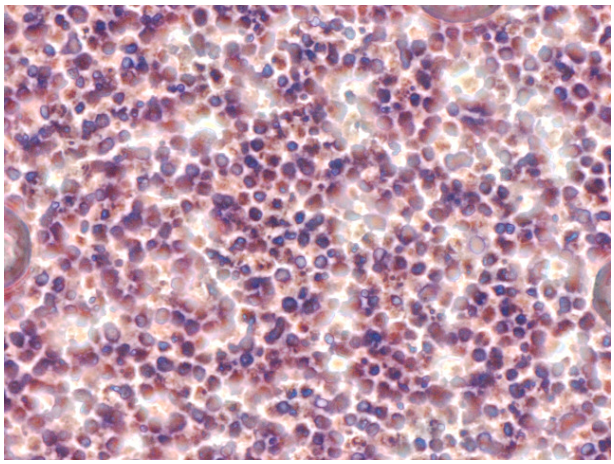

Fig. 4.9: Unlabeled NK-92-scFv(FRP5)-ζ cells with nuclear fast red counterstain.

NK-92-scFv(FRP5)-mζ cells

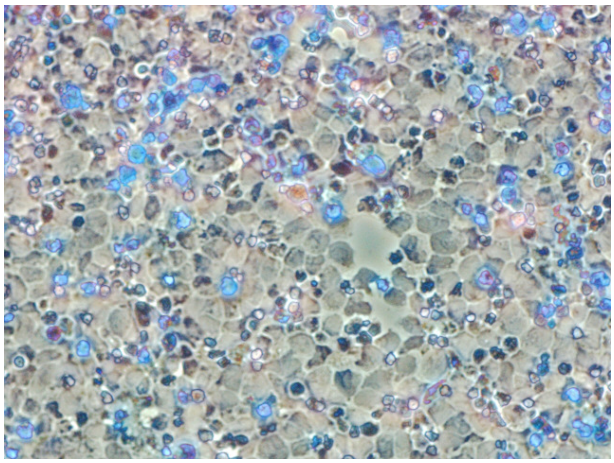

Fig. 4.10: NK-92-scFv(FRP5)-mζ cells were also fixed and labeled with Prussian Blue stain. The presence of iron in the cells is demonstrated by the blue tinge. The adequate labeling of the cells is proved.

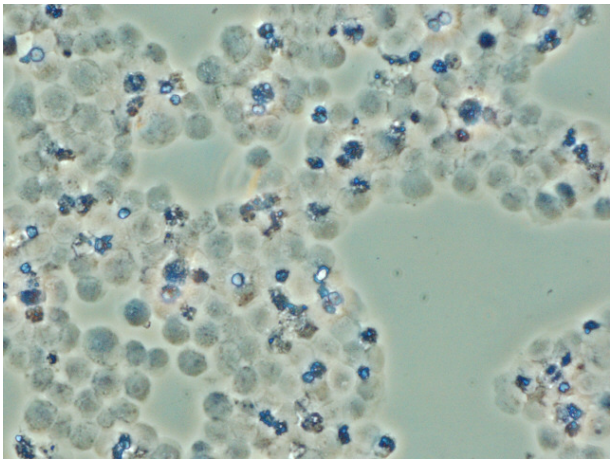

Fig. 4.11: Unlabeled NK-92-scFv(FRP5)-mζ cells just as the aforementioned unlabeled NK cells stained with Prussian Blue do not show any blue staining which would indicate the presence of intracellular iron.

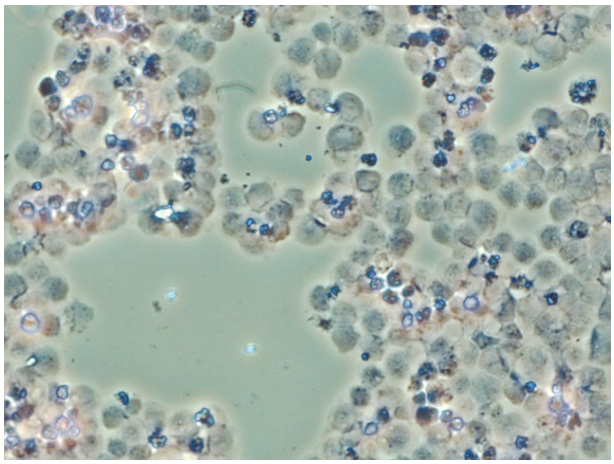

Fig. 4.12: Unlabeled NK-92-scFv(FRP5)-mζ cells with nuclear fast red counterstain.

To summarize, all NK cells incorporated Endorem very well after adding Lipofectin to the ferumoxide cell-suspension composite. However, the pictures provided above show that there are slight differences in the intensity of the staining of the different NK cells.

4.1.3 Analysis of Representative Chimeric Antigen Receptor Expression

EpCAM-expression in DU-145, PC-3, LNCaP

In the following three images of the Flow Cytometry analysis, EpCAM-expression in DU-145, PC-3 and LNCaP cells is demonstrated. The unfilled graphs outline staining with an EpCAM-specific antibody while the black graphs represent staining with an isotype control.

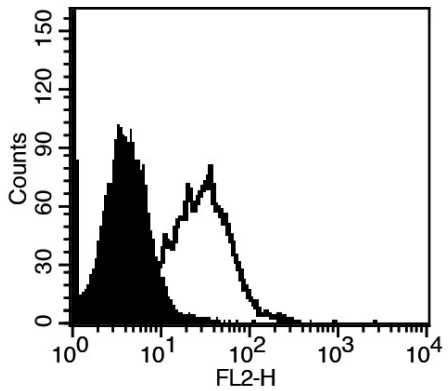

Fig. 4.13: EpCAM-expression in PC-3

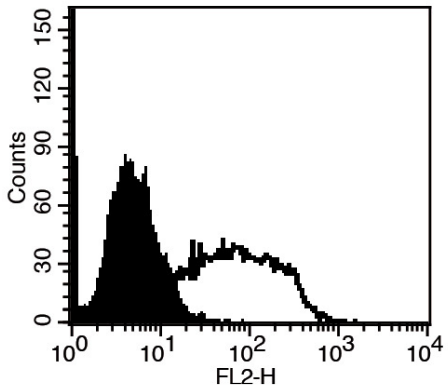

Fig. 4.14: EpCAM-expression in DU-145

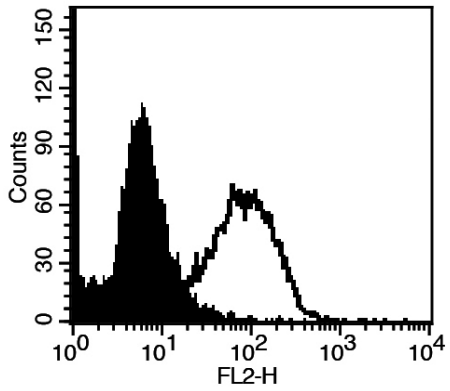

Fig. 4.15: EpCAM-expression in LNCaP

To summarize, the different prostate cancer cells all express EpCAM distinctly.

ErbB2- and EpCAM-Expression in MDA-MB-453

The next two images (fig. 4.16 and fig. 4.17) show the Flow Cytometry analysis of EpCAM and ErbB2-expression in MDA-MB-453 cells. The unfilled graph presents staining with an EpCAM- or an ErbB2-specific antibody while the gray graph presents staining with an isotype control.

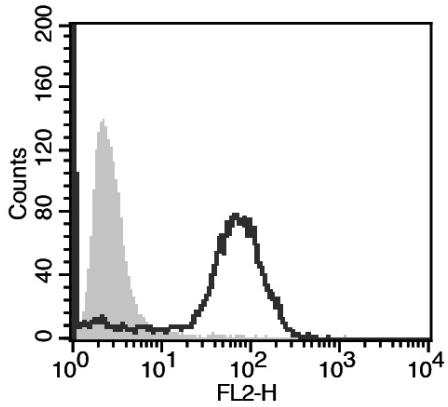

Fig 4.16: EpCAM-expression in MDA-MB-453

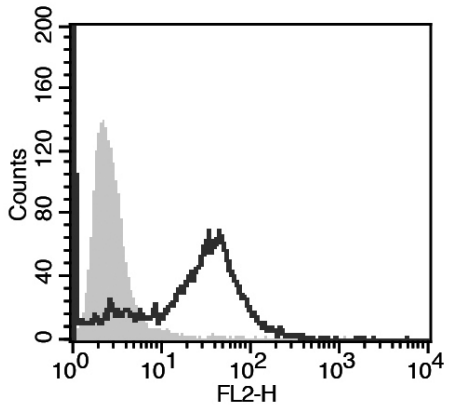

Figure 4.17: ErbB2-expression in MDA-MB-453

All in all the EpCAM- and the ErbB2-expression is approximately equal in this assay.

Anti-EpCAM specificity in NK-92-scFv(MOC31)-ζ

Flow cytometry analysis of anti-EpCAM specifity in NK-92-scFv(MOC31)-ζ cells is demonstrated in the following image (fig. 4.18). The unfilled, black framed graph represents staining of NK-92-scFv(MOC31)-ζ cells with the Myc-tag specific monoclonal antibody 9E10 while the gray graph represents untargeted NK-92 control cells.

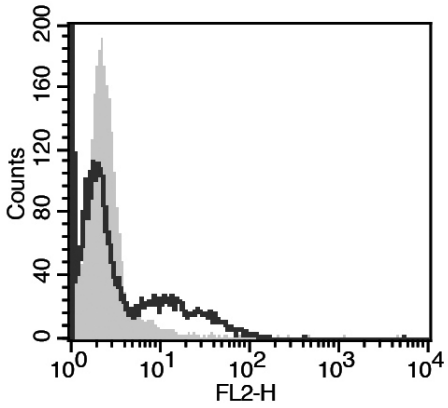

Fig. 4.18: Anti-EpCAM specificity in NK-92-scFv(MOC31)-ζ

Anti-EpCAM specificity in NK-92-scFv(FRP5)-ζ

The image below (fig. 4.19) shows the Flow Cytometry analysis of Anti-EpCAM specificity in NK-92-scFv(FRP5)-ζ. The unfilled, black framed graph demonstrates staining of NK-92-scFv(FRP5)-ζ cells with the Myc-tag specific monoclonal antibody 9E10 while the gray graph demonstrates untargeted NK-92 control cells.

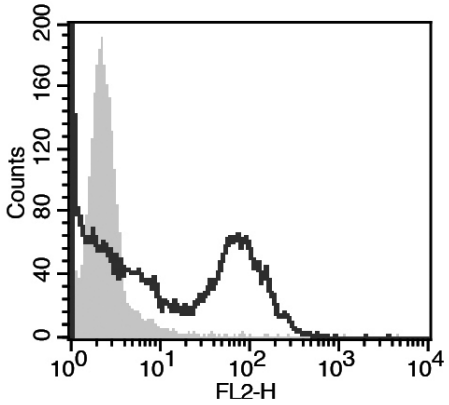

Fig. 4.19: Anti-EpCAM specificity in NK-92-scFv(FRP5)-ζ

All in all both NK-cell lines, NK-92-scFv(MOC31)-ζ and NK-92-scFv(FRP5)-ζ are specific for anti-EpCAM-expression.

4.1.4 Cytotoxicity Assays

Prostate Cancer Cells – Unlabeled NK Cells

DU-145

A) Specific cell killing of unlabeled NK-92-scFv(MOC31)-ζ towards DU-145 in comparison to unspecific cell killing of unlabeled NK-92

Fig. 4.20 shows the specificity of target cell recognition and enhanced cytotoxicity of EpCAM-specific NK-92-scFv(MOC31)-ζ cells towards EpCAM-expressing DU-145 prostate carcinoma cells. DU-145 cells were stained with CFSE before they were incubated with unmodified parental NK-92 or EpCAM-specific NK-92-scFv(MOC31)-ζ cells at an effector to target ratio of 1:1, 5:1 and 10:1 for 2 hours. Propidium iodide was added and subsequently the relative number of dead target cells was determined as double positive cells by flow cytometry. EpCAM-expressing DU-145 cells are specifically lysed by NK-92-scFv(MOC31)-ζ cells in comparison to parental NK-92 cells as the effector to target ratios are 15.68/10.63, 27.54/9.77 and 42.23/15.02.

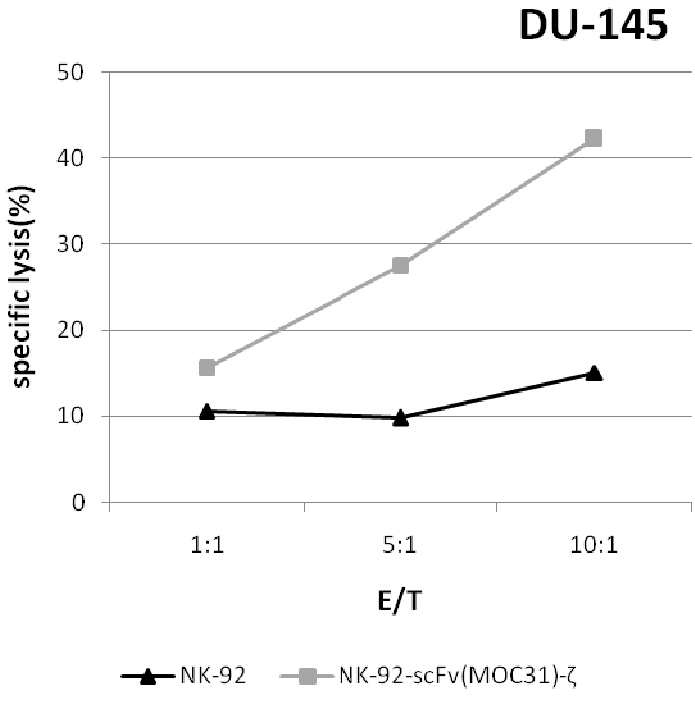

Fig. 4.20

B) Specific cell killing of unlabeled NK-92-scFv(FRP5)-mζ towards DU-145 in comparison to unspecific cell killing of unlabeled NK-92

Fig. 4.21 demonstrates the specificity of target cell recognition and enhanced cytotoxicity of ErbB2-specific NK-92-scFv(FRP5)-mζ cells towards ErbB2-expressing DU-145 prostate carcinoma cells. DU-145 cells were stained with CFSE in the same manner as described in A) before they were incubated with unmodified parental NK-92 or ErbB2-specific NK-92-scFv(FRP5)-mζ cells at the same effector to target ratio of 1:1, 5:1 and 10:1 for 2 hours as in A). Propidium iodide was added and the relative number of dead target cells was determined as double positive cells by flow cytometry. ErbB2-expressing DU-145 cells are specifically lysed by NK-92-scFv(FRP5)-mζ cells in comparison to parental NK-92 cells as the effector to target ratios are 13.11/10.63, 19.62/9.77 and 39.41/15.02.

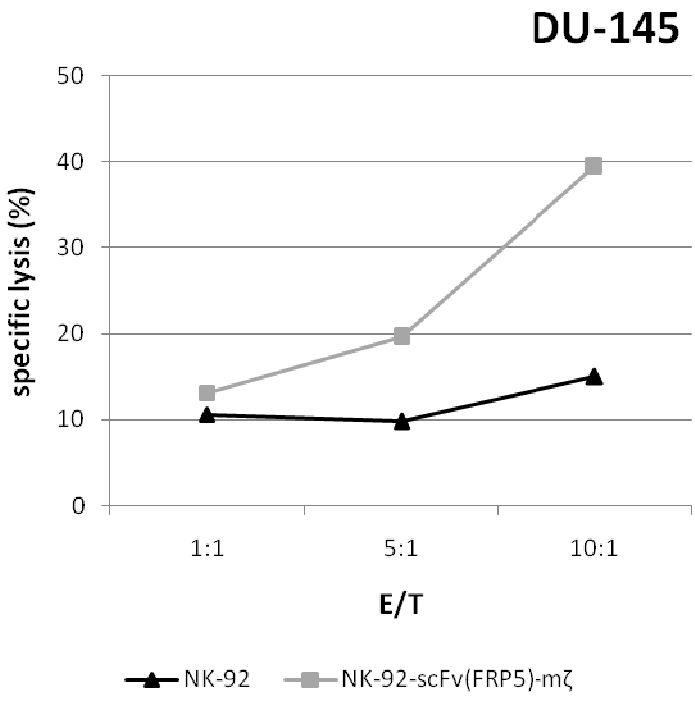

Fig. 4.21

PC-3

C) Specific cell killing of unlabeled NK-92-scFv(MOC31)-ζ towards PC-3 in comparison to unspecific cell killing of unlabeled NK-92

The specificity of target cell recognition and enhanced cytotoxicity of EpCAM-specific PC-3 prostate carcinoma cells is demonstrated in fig. 4.22. PC-3 cells were stained with CFSE before they were incubated with unmodified parental NK-92 or EpCAM-specific NK-92-scFv(MOC31)-ζ cells at an effector to target ratio of 1:1, 5:1 and 10:1 for 2 hours. Propidium iodide was added and subsequently the relative number of dead target cells was determined as double positive cells by flow cytometry. EpCAM-expressing PC-3 cells are specifically lysed by NK-92-scFv(MOC31)-ζ cells in comparison to parental NK-92 cells as the effector to target ratios are 39.35/38.54, 51.42/35.87 and 59.97/32.49.

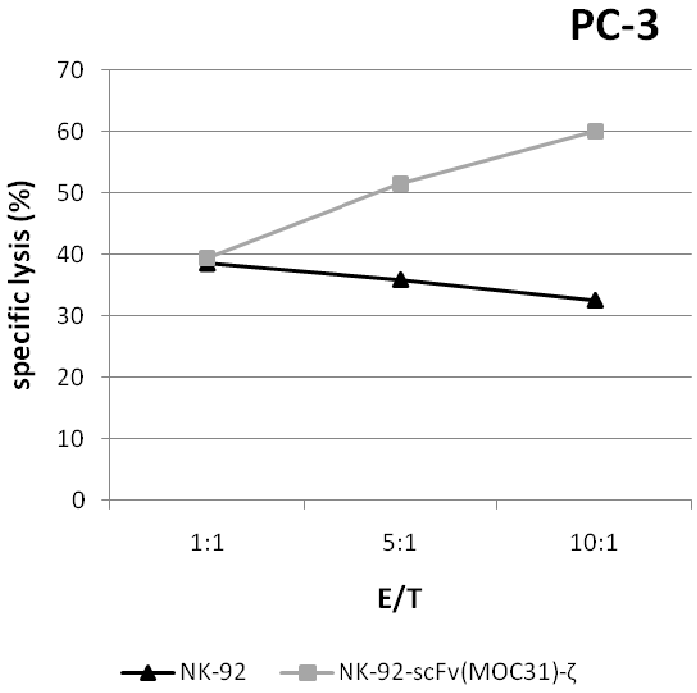

Fig. 4.22

D) Specific cell killing of unlabeled NK-92-scFv(FRP5)-mζ towards PC-3 in comparison to unspecific cell killing of unlabeled NK-92

Fig. 4.23 displays the specificity of target cell recognition and enhanced cytotoxicity of ErbB2-specific PC-3 prostate carcinoma cells. PC-3 cells were stained with CFSE just as in C) before they were incubated with unmodified parental NK-92 or ErbB2-specific NK-92-scFv(FRP5)-mζ cells at an effector to target ratio of 1:1, 5:1 and 10:1 for 2 hours. Propidium iodide was also added and the relative number of dead target cells was determined as double positive cells by flow cytometry. ErbB2-expressing PC-3 cells are specifically lysed by NK-92-scFv(FRP5)-mζ cells in comparison to parental NK-92 cells only at an effector to target ratio of 10:1 as the effector to target ratios are 31.92/38.54, 31.85/35.87 and 40.34/32.49.

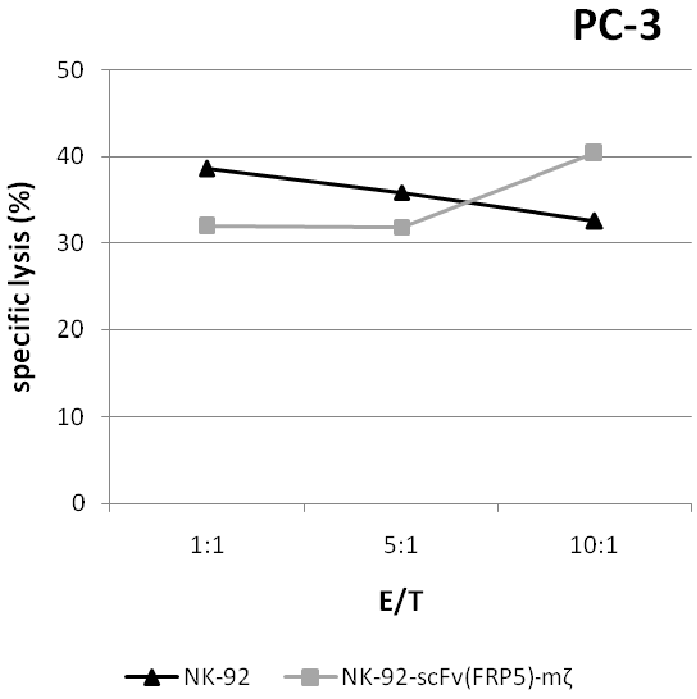

Fig. 4.23

LNCaP

E) Specific cell killing of unlabeled NK-92-scFv(MOC31)-ζ towards LNCaP in comparison to unspecific cell killing of unlabeled NK-92

In fig. 4.24 the specificity of target cell recognition and enhanced cytotoxicity of EpCAM-specific LNCaP prostate carcinoma cells is shown. LNCaP cells were stained with CFSE before they were incubated with unmodified parental NK-92 or EpCAM-specific NK-92-scFv(MOC31)-ζ cells at an effector to target ratio of 1:1, 5:1 and 10:1 for 2 hours. Propidium iodide was added and subsequently the relative number of dead target cells was determined as double positive cells by flow cytometry. EpCAM-expressing LNCaP cells are specifically lysed by NK-92-scFv(MOC31)-ζ cells in comparison to parental NK-92 cells as the effector to target ratios are 31.40/33.25, 52.99/33.00 and 62.70/33.42.

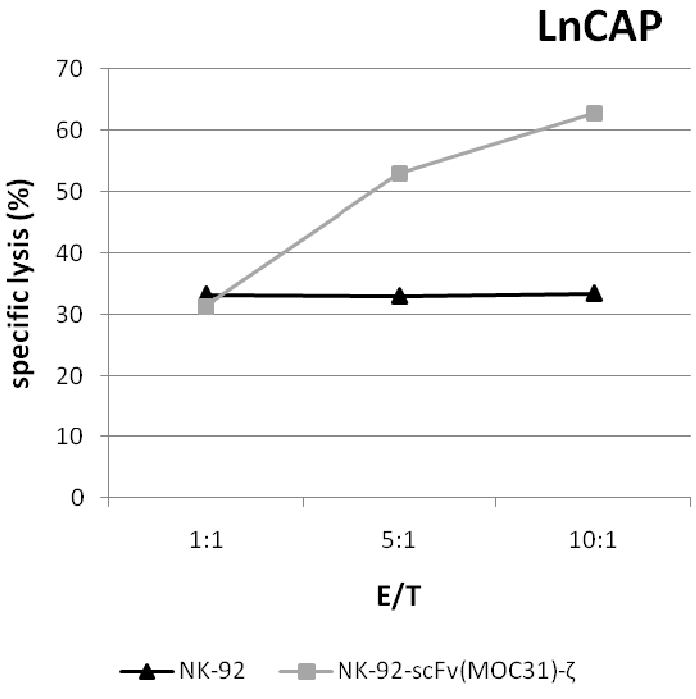

Fig. 4.24

F) Specific cell killing of unlabeled NK-92-scFv(FRP5)-mζ towards LNCaP in comparison to unspecific cell killing of unlabeled NK-92

Fig. 4.25 demonstrates the specificity of target cell recognition and enhanced cytotoxicity of ErbB2-specific LNCaP prostate carcinoma cells. In the exact same manner as in E) LNCaP cells were stained with CFSE before they were incubated with unmodified parental NK-92 or ErbB2-specific NK-92-scFv(FRP5)-mζ cells at an effector to target ratio of 1:1, 5:1 and 10:1 for 2 hours. Propidium iodide was also added and subsequently the relative number of dead target cells was determined as double positive cells by flow cytometry. ErbB2-expressing LNCaP cells are specifically lysed by NK-92-scFv(FRP5)-mζ cells in comparison to parental NK-92 cells as the effector to target ratios are 30.40/33.25, 46.33/33.00 and 55.93/33.42.

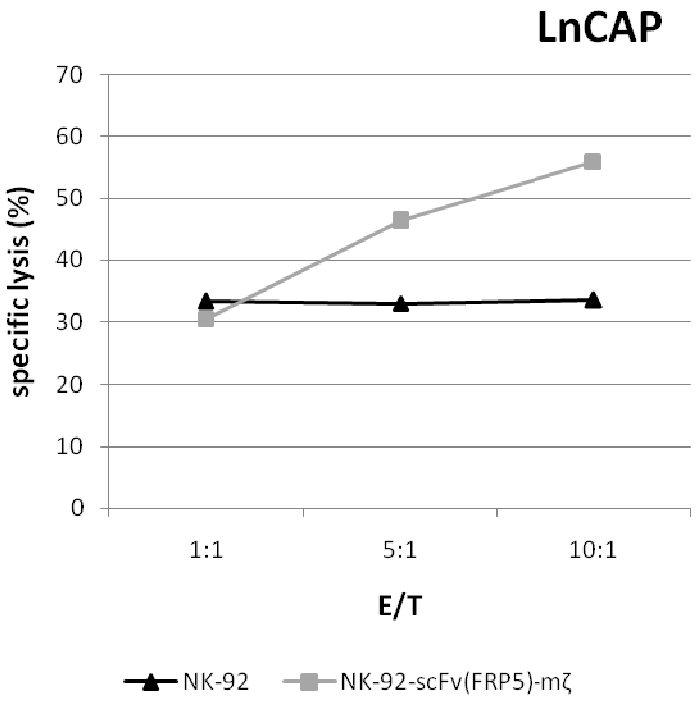

Fig. 4.25

Breast Cancer Cells – Unlabeled NK cells

MDA-MB-453

G) Specific cell killing of unlabeled NK-92-scFv(FRP5)-ζ towards MDA-MB-453 in comparison to unspecific cell killing of unlabeled NK-92

Fig. 4.26 demonstrates the specificity of target cell recognition and enhanced cytotoxicity of ErbB2-specific NK-92-scFv(FRP5)-ζ cells towards ErbB2-expressing MDA-MB-453 breast carcinoma cells. MDA-MB-453 cells were stained with CFSE before they were incubated with unmodified parental NK-92 or ErbB2-specific NK-92-scFv(FRP5)-ζ cells at an effector to target ratio of 1:1, 10:1 and 20:1 for 2 hours. Propidium iodide was added and subsequently the relative number of dead target cells was determined as double positive cells by flow cytometry. ErbB2-expressing MDA-MB-453 cells are specifically lysed by NK-92-scFv(FRP5)-ζ cells in comparison to parental NK-92 cells as the effector to target ratios are 37.97/19.54, 66.74/16.58 and 71.97/13.25.

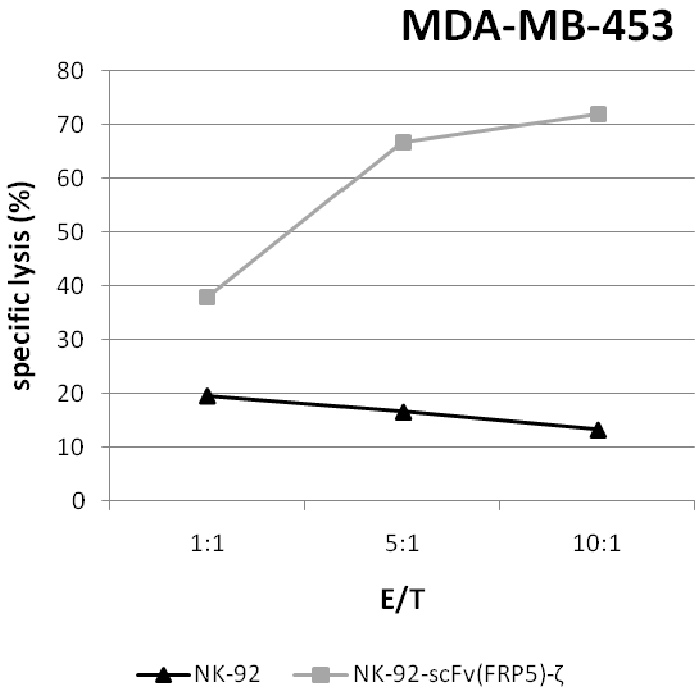

Fig. 4.26

MCF-7

H) Specific cell killing of unlabeled NK-92-scFv(FRP5)-ζ towards MCF-7 in comparison to unspecific cell killing of unlabeled NK-92

In fig. 4.27 the specificity of target cell recognition and enhanced cytotoxicity of ErbB2-specific NK-92-scFv(FRP5)-ζ cells towards ErbB2-expressing MCF-7 breast carcinoma cells is shown. As in H), MCF-7 cells were stained with CFSE before they were incubated with unmodified parental NK-92 or ErbB2-specific NK-92-scFv(FRP5)-ζ cells at an effector to target ratio of 1:1, 5:1 and 10:1 for 2 hours. Propidium iodide was added and subsequently the relative number of dead target cells was determined as double positive cells by flow cytometry. ErbB2-expressing MCF-7 cells are not specifically lysed by NK-92-scFv(FRP5)-ζ cells in comparison to parental NK-92 cells as the effector to target ratios are 38.95/48.77, 31.74/44.54 and 42.75/39.43. At the effector to target ratio of 10:1 the specific lysis caused by NK-92-scFv(FRP5)-ζ cells is higher than the one caused by parental NK-cells but not significally. Higher effector to target ratio would have to be tested.

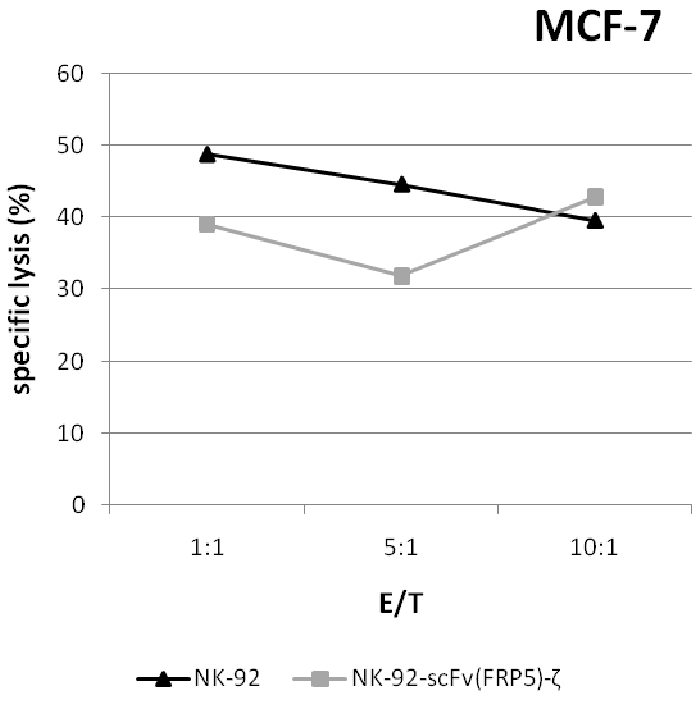

Fig. 4.27

Breast Cancer Cells – Labeled NK cells

MCF-7

I) Specific cell killing of labeled NK-92-scFv(FRP5)-ζ towards MCF-7 in comparison to unspecific cell killing of labeled NK-92

Fig. 4.28 visualizes the specificity of target cell recognition and enhanced cytotoxicity of labeled ErbB2-specific NK-92-scFv(FRP5)-ζ cells towards ErbB2-expressing MCF-7 breast carcinoma cells. MCF-7 cells were stained with CFSE before they were incubated with labeled unmodified parental NK-92 or labeled ErbB2-specific NK-92-scFv(FRP5)-ζ cells at an effector to target ratio of 1:1, 5:1 and 10:1 for 2 hours. Propidium iodide was added and subsequently the relative number of dead target cells was determined as double positive cells by flow cytometry. ErbB2-expressing MCF-7 cells are not specifically lysed by labeled NK-92-scFv(FRP5)-ζ cells in comparison to labeled parental NK-92 cells as the effector to target ratios are 29.77/36.58, 29.65/37.23 and 27.66/40.05.

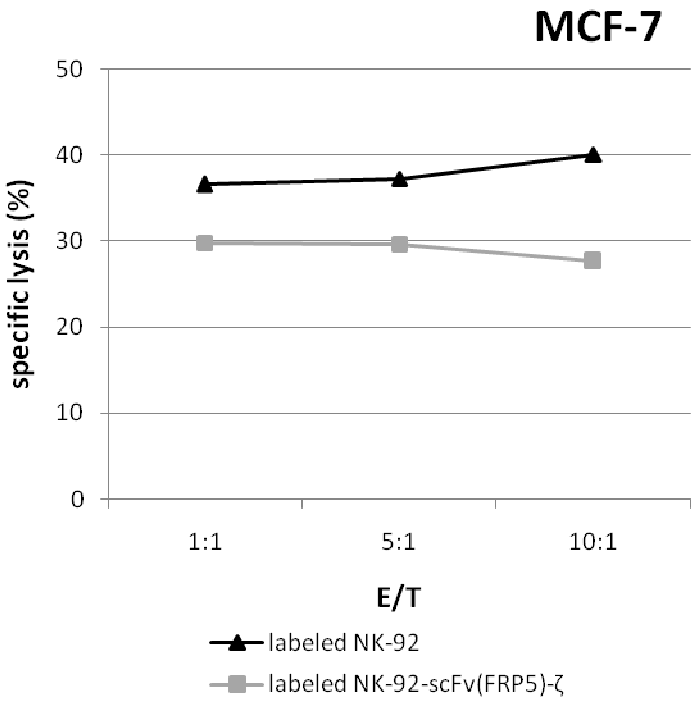

Fig. 4.28

		E/T Ratio		
Unlabeled Effector	**Target**	**1:1**	**5:1**	**10:1**
NK-92	DU-145	10.63	9.77	15.02
NK-92-scFv(MOC31)-ζ		15.68	27.54	42.23
NK-92-scFv(FRP5)-mζ		13.11	19.62	39.41
NK-92	PC-3	38.54	35.87	32.49
NK-92-scFv(MOC31)-ζ		39.35	51.42	59.97
NK-92-scFv(FRP5)-mζ		31.92	31.85	40.34
NK-92	LNCaP	33.25	33.00	33.42
NK-92-scFv(MOC31)-ζ		31.40	52.99	62.70
NK-92-scFv(FRP5)-mζ		30.40	46.33	55.93
NK-92	MDA-MB-453	19.54	16.58	13.25
NK-92-scFv(FRP5)-ζ		37.97	66.74	71.97
NK-92	MCF-7	48.77	44.54	39.43
NK-92-scFv(FRP5)-ζ		38.95	31.74	42.75

Table 4.1: Unlabeled effector to target ratio of parental NK-92 cells or genetically modified NK cells to prostate cancer cells or breast cancer cell lines

Labeled Effector	**Target**	**1:1**	**5:1**	**10:1**
NK-92	MCF-7	36.58	37.23	40.05
NK-92-scFv(FRP5)-ζ		29.77	29.65	27.66

Table 4.2: Labeled effector to target ratio of parental NK-92 cells (A-C) or NK-92-scFv(FRP5)-ζ cells to MCF-7 cells

Reference cell line K562

Preservation of cytotoxicity of the NK Cell Lines NK-92, NK-92-scFv(FRP5)-ζ, NK-92-scFv(MOC31)-ζ and NK-92-scFv(FRP5)-mζ towards K562

Fig. 4.29 to 4.32 show the preservation of cytotoxicity after labeling NK cells with ferumoxides. Unspecific parental NK-92 cells, ErbB2-specific NK-92-scFv(FRP5)-ζ cells, EpCAM-specific NK-92-scFv(MOC31)-ζ and ErbB2-specific NK-92-scFv(FRP5)-mζ cells were labeled with ferumoxides before incubation with K562 cells as targets. Cytotoxic activity of unlabeled parental NK-92 cells, NK-92-scFv(FRP5)-ζ cells, NK-92-scFv(MOC31)-ζ and NK-92-scFv(FRP5)-mζ cells is shown for comparison. The charts show that the cytotoxicity was not affected by labeling the cells as the effector to target ratios are very close to each other (tab. 4.3). The FACS-based cytotoxicity assay was performed as decribed above.

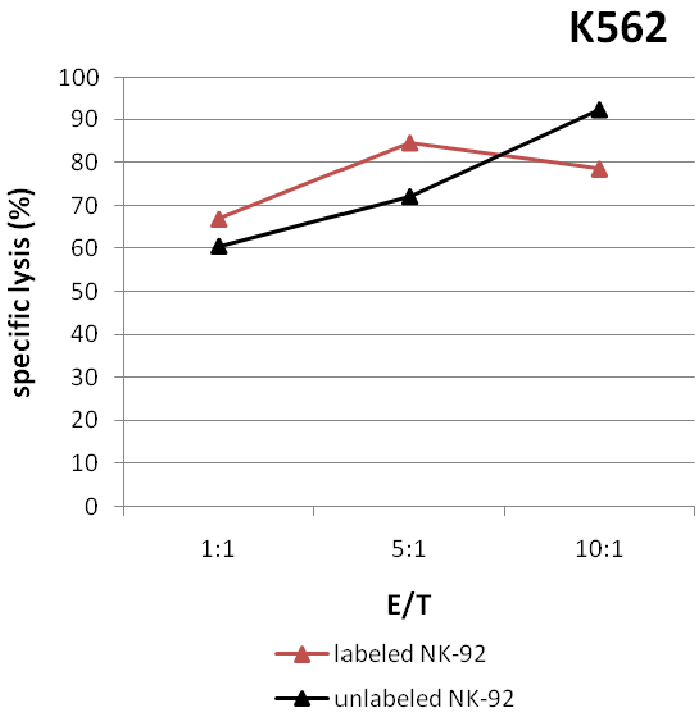

Fig. 4.29

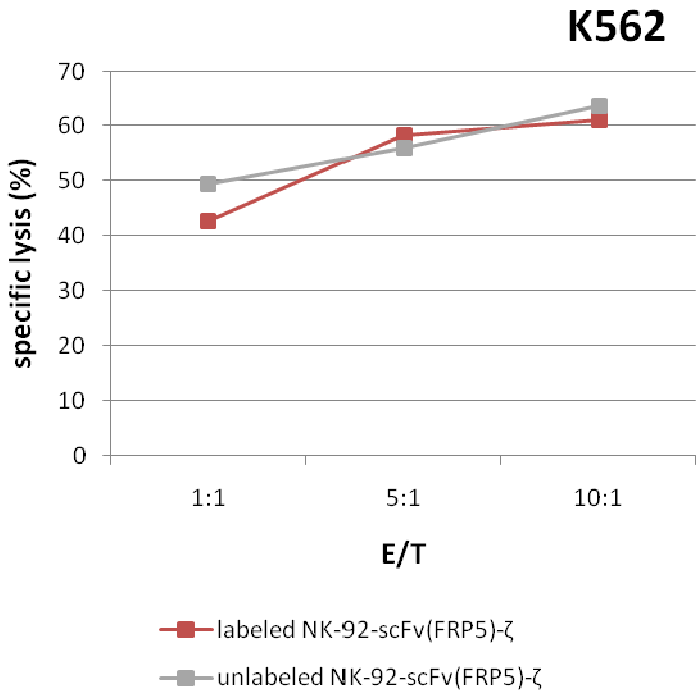

Fig. 4.30

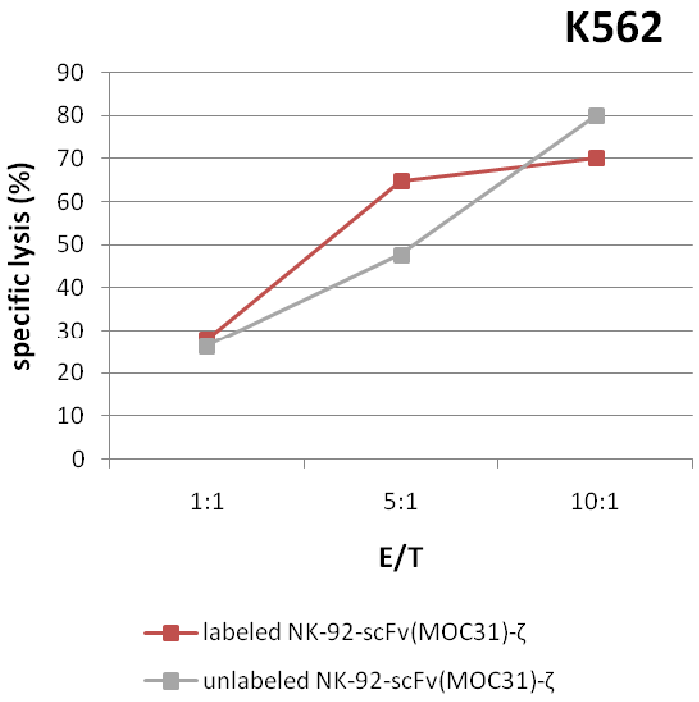

Fig. 4.30

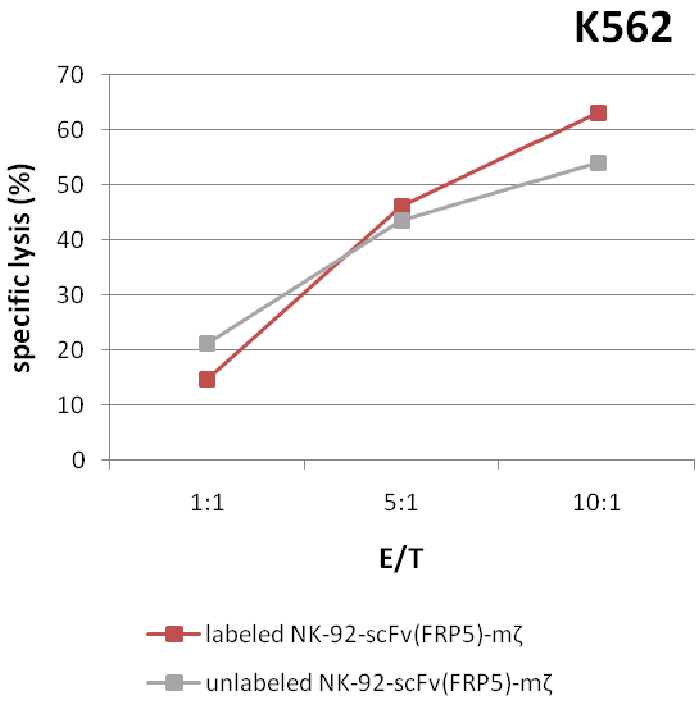

Fig. 4.32

		E/T Ratio		
Effector		**1:1**	**5:1**	**10:1**
Parental NK-92	unlabeled	60.56	72.13	92.34
	labeled	66.88	84.47	78.48
NK-92-scFv(FRP5)-ζ	unlabeled	49.40	55.85	63.44
	labeled	42.70	58.26	60.98
NK-92-scFv(MOC31)-ζ	unlabeled	26.34	47.63	79.84
	labeled	27.99	64.72	70.09
NK-92-scFv(FRP5)-mζ	unlabeled	21.34	43.55	53.92
	labeled	14.80	46.24	63.12

Table 4.3: NK cells incubated with K562 cells

4.2 In Vivo Studies

4.2.1 OI Scan with Genetically Modified NK-92-scFv(MOC31)-ζ Cells

DU-145 prostate cancer cells which are EpCAM-positive were implanted into all 12 rats. Six of them received an injection of DiD-labeled NK-92-scFv(MOC31)-ζ cells into their tail vein (fig. 4.33-4.38). Optical imaging scans were obtained before and at 1.5 hours, 8 hours and 24 hours after the injection of genetically modified NK-92-scFv(MOC31)-ζ cells. On the optical imaging scans a marked tumor fluorescence post injection was observed. Quantitative fluorescence signal intensity data of the tumors were significantly higher on postinjection than in preinjection scans at all investigated time points ($p<0.05$). An increase of the fluorescence on the optical imaging scans at 1.5 hours and 8 hours was determined. In the last scan, at 24 hours, the fluorescence had leveled off. In the pre-injection scan the green arrow is pointing to the tumor. In the 1.5 hours as well as in the 8 hours postinjection scan a signal within the tumor as well as in the liver is detected. In the last image, at 24 hours after the NK-92-scFv(MOC31)-ζ cell injection, the main signal intensity is determined within the tumor not the liver.

	Fig. 4.33	Fig. 4.34
Pre-injection scan	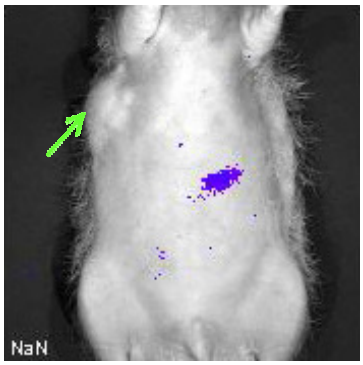	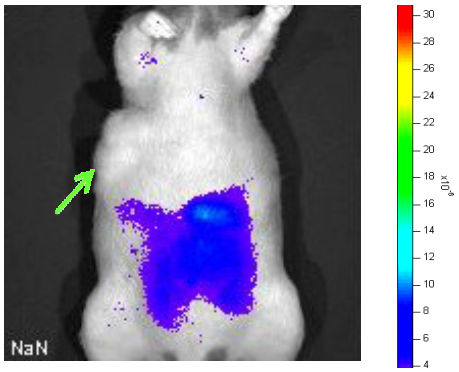
1.5 hrs post injection	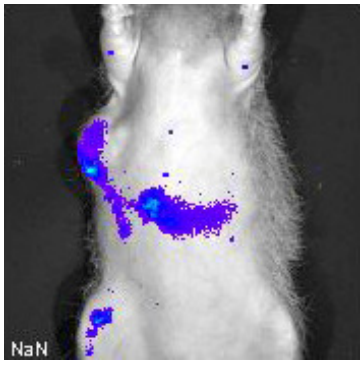	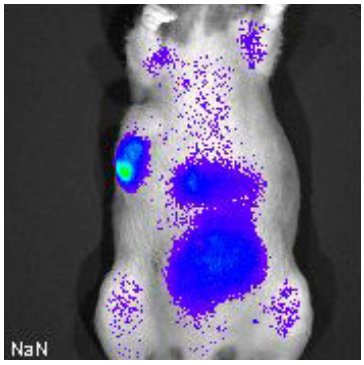
8 hrs p.i.	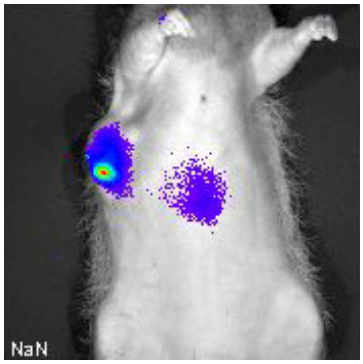	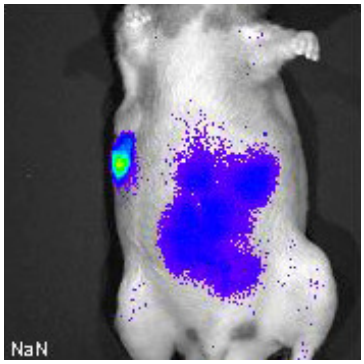
24 hrs p.i.	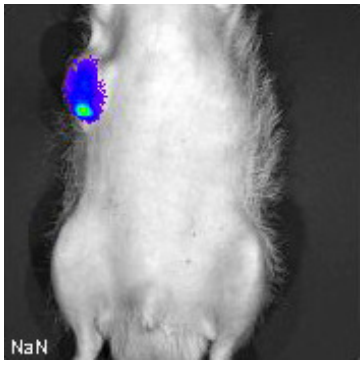	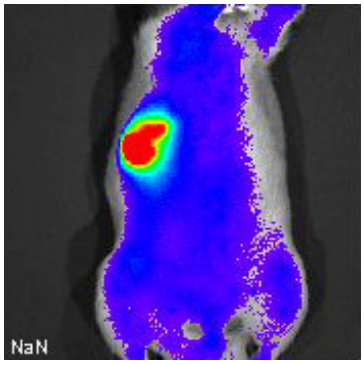

	Fig. 4.35	Fig. 4.36
Pre-injection scan	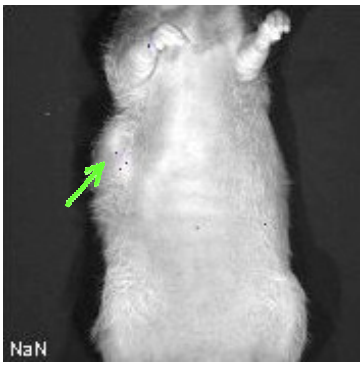	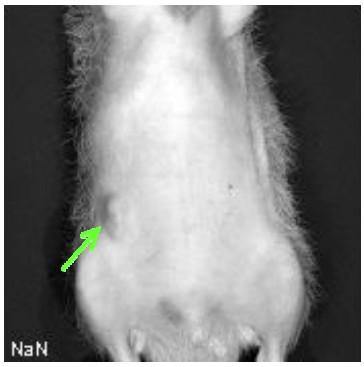
1.5 hrs post injection	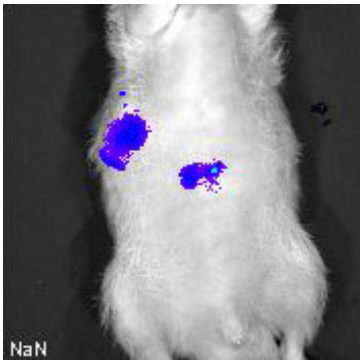	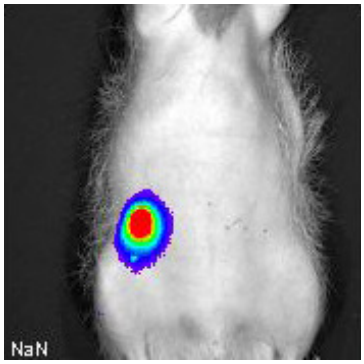
8 hrs p.i.	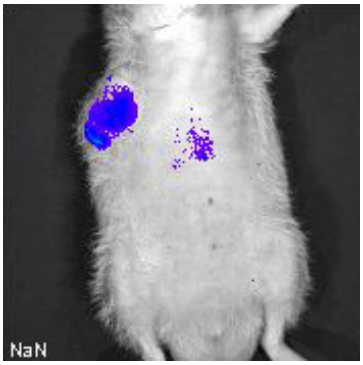	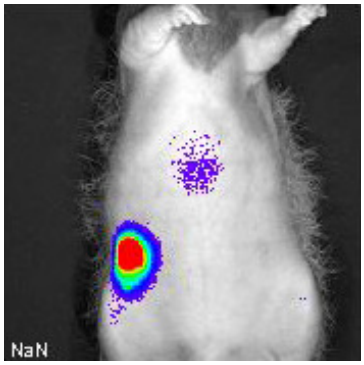
24 hrs p.i.	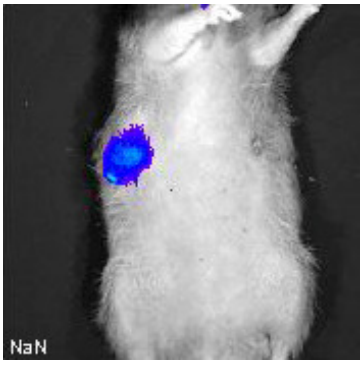	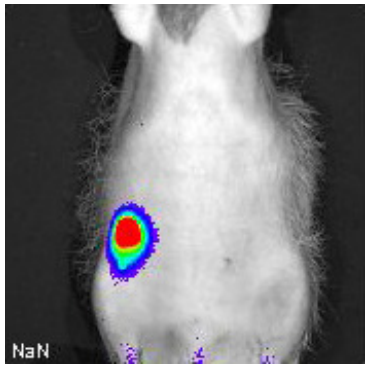

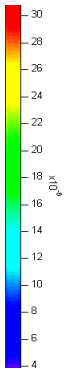

	Fig. 4.37	Fig. 4.38
Pre-injection scan	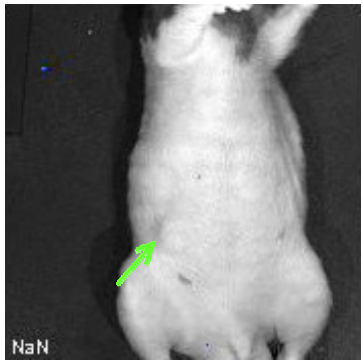	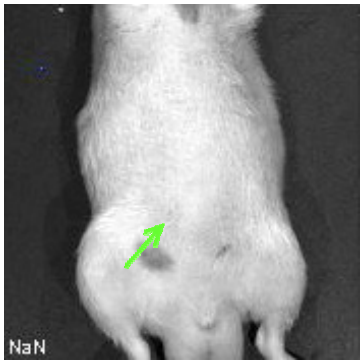
1.5 hrs post injection	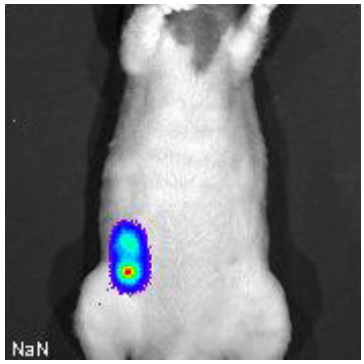	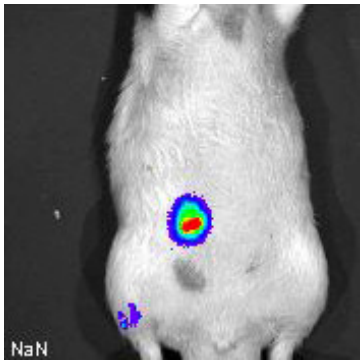
8 hrs p.i.	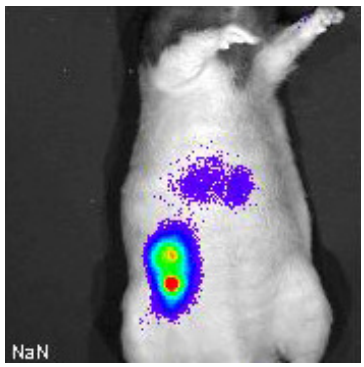	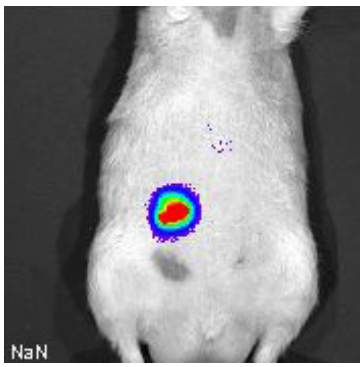
24 hrs p.i.	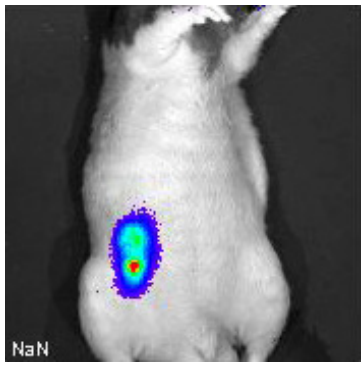	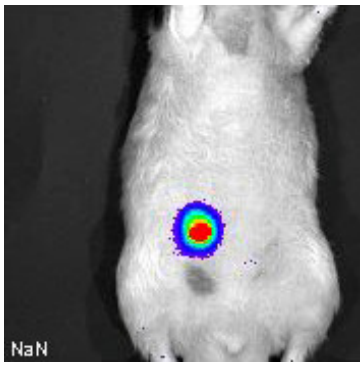

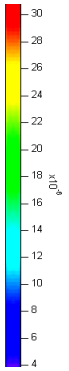

4.2.2 OI Scan with Parental NK-92 Cells

The EpCAM-positive DU-145 prostate cancer cells were also implanted into the other six rats. However, these rats received an injection of DiD-labeled parental NK-92 cells into their tail vein. In fig. 4.39 the serial optical imaging of one representative of the rats is displayed. At no scanning time of the representative rat a fluorescent signal could be determined in the tumor (green arrow). The fluorescence signal of the tumors on postinjection scans showed no significant increase in comparison to preinjection scans at all times ($p<0.05$). Merely at 1.5 hours post injection and 24 hours post injection cellular accumulation was assessed in the liver (black arrow).

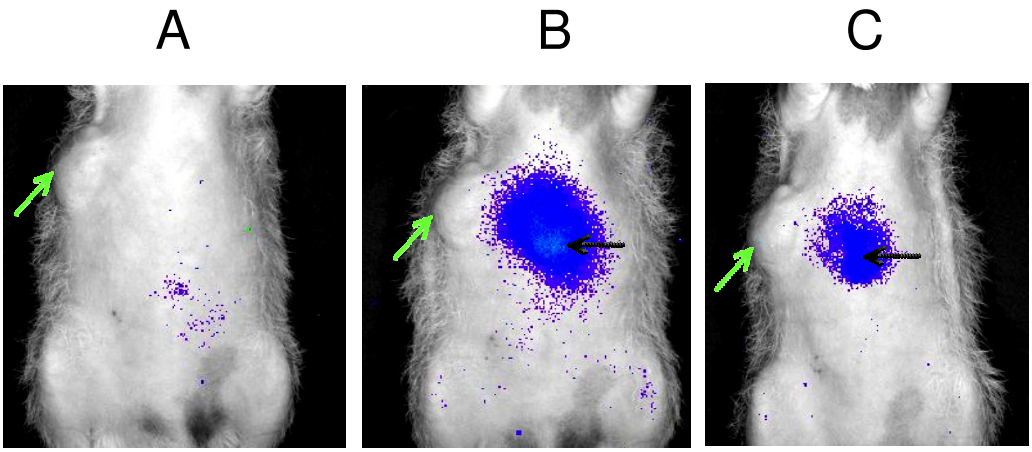

Fig. 4.39: Representative rat injected with parental NK-92 cells

The tumor fluorescence after injection of NK-92-scFv(MOC31)-ζ cells was significantly higher in comparison to the tumor fluorescence after injection of parental NK-92 cells ($p<0.05$).

Fig. 4.40 shows the quantitative in vivo analysis of the tumor fluorescence. A significant increase in the signal intensity of the tumor fluorescence is confirmed after injection of NK-92-scFv(MOC31)-ζ cells in comparison with preinjection scans. After injection of parental NK cells the fluorescence signal of control

tumors is unchanged. Data are illustrated as means of six animals in each group with standard deviations. The three asterisks show the significant difference between the fluorescence signal of animals that received NK-92-scFv(MOC31)-ζ cells or NK-92 parental cells ($p<0.05$).

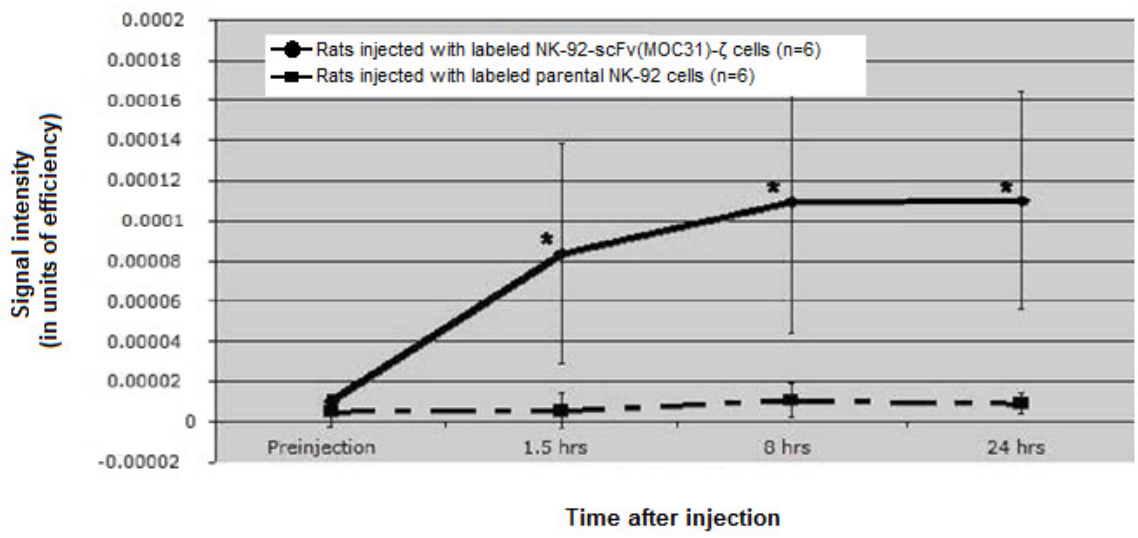

Fig. 4.40: Quantitative in vivo analysis

4.2.3 Ex Vivo OI scan

In fig. 4.41 the ex vivo optical imaging study of two representative rats is presented. The upper image shows the explanted tumors and organs of a representative rat 24 hours after injection of NK-92-scFv(MOC31)-ζ cells. The distinct fluorescence of the tumor in comparison to the explanted organs is clearly recognizable. The lower image shows the explanted tumors and organs of a representative rat 24 hours after injection of parental NK-92 cells. The tumor did not demonstrate any increased fluorescence in comparison to the organs. The fluorescence intensity of the ex vivo tumors of the NK-92-scFv(MOC31)-ζ group was significantly higher than of the NK parental group ($p<0.05$, n=6 in each group). Legend: T=tumor, Li=liver, Sp=spleen, Lu=lungs, St=sternum).

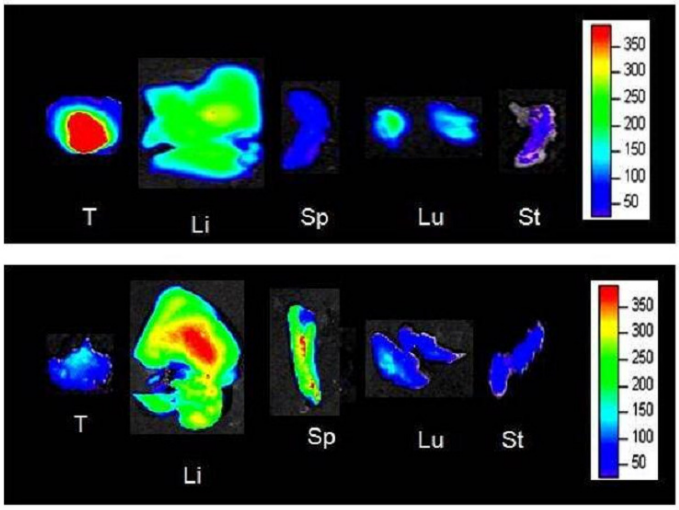

Fig. 4.41: Ex vivo optical imaging

In fig. 4.42 the quantitative ratio of tumor to organ fluorescence at 24 hours postinjection of NK-92-scFv(MOC31)-ζ cells (black bars) or NK-92 cells (patterned bars) is demonstrated. Data are illustrated as means of six animals in each group with standard deviations. The three asterisks show the significant difference between the fluorescence signal of animals that received NK-92-scFv(MOC31)-ζ cells or NK-92 parental cells ($p<0.05$).

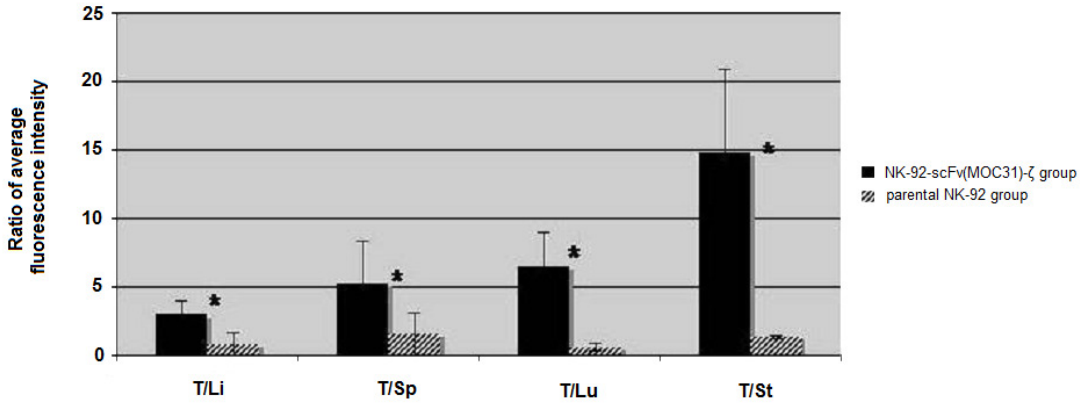

Fig. 4.42: Quantitative ratio of tumor to organ fluorescence at 24 hours postinjection of NK-92-scFv(MOC31)-ζ cells (black bars) or parental NK-92 cells (patterned bars)

4.2.4 Fluorescence Microscopy

Fluorescence microscopy was conducted in order to confirm the accumulation of NK-92-scFv(MOC31)-ζ cells in the tumors at 24 hours post injection in comparison to the absence of the parental NK-92 cells in the tumors (fig. 4.43). In image A, DiD labeled NK-92-scFv(MOC31)-ζ cells are depicted in the tumor tissue with the Cy5 (red) channel. Image B also shows the occurrence of NK-92-scFv(MOC31)-ζ cells by anti-CD 94 immunostaining conjugated with FITC in the green channel as this staining is specific for human NK cells. Using an overlay of the images of DiD and FITC labeled NK-92-scFv(MOC31)-ζ cells Image C confirms that the DiD-containing cells are indeed the applied NK-92-scFv(MOC31)-ζ cells (red and green channel). Image D shows that the tumors of the control group which received parental NK-92 cells do not demonstrate any NK cell accumulation.

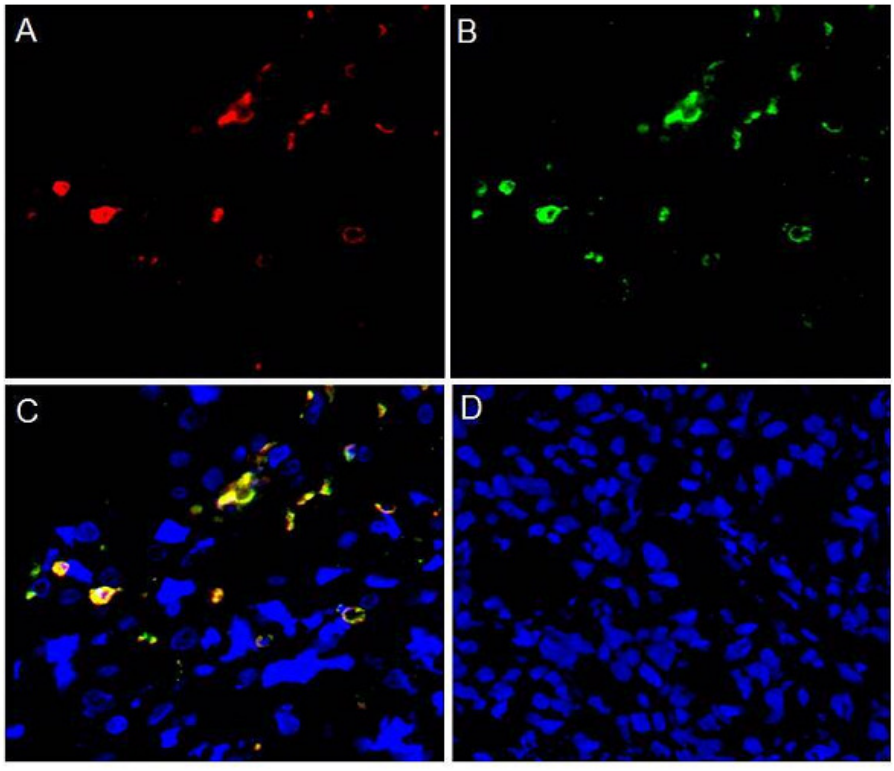

Fig. 4.43: Confocal microscopy of a representative tumor at 24 hours after the injection of NK-92-scFv(MOC31)-ζ cells (A-C) or parental NK-92 cells

5 Discussion

The objectives of this thesis were to label the different NK cells with the ferumoxide Endorem or the fluorochrome DiD in order to visualize the cells in the MRI or the optical imaging and to confirm the cytotoxicity of the cells.

The data collected in this thesis demonstrate in various in vitro cytotoxicity assays the specificity of target cell recognition and enhanced cytotoxicity of genetically modified NK cells: EpCAM-specific NK-92-scFv(MOC31)-ζ, ErbB2-specific NK-92-scFv(FRP5)-mζ and NK-92-scFv(FRP5)-ζ are tested towards DU-145, PC-3 and LnCAP cells or MCF-7 and MDA-MB-453 cells. In comparison to the modified cells parental NK-92 cells that do not specifically lyse prostate or breast carcinoma cells are also tested. For the in vitro analysis the cells were labeled with the ferumoxide Endorem. In order to confirm the specific and efficient killing of prostate or breast cancer cells by genetically modified NK-92 cells several flow cytometry–based cytotoxicity assays were performed (see fig. 4.20-4.28): DU-145 cells are specifically lysed by NK-92-scFv(MOC31)-ζ cells and by NK-92-scFv(FRP5)-mζ cells; PC-3 cells are specifically lysed by NK-92-scFv(MOC31)-ζ cells and by NK-92-scFv(FRP5)-mζ cells; LNCaP cells are specifically lysed by NK-92-scFv(MOC31)-ζ cells and by NK-92-scFv(FRP5)-mζ cells; MDA-MB-453 cells are specifically lysed by NK-92-scFv(FRP5)-ζ cells. MCF-7 cells are not specifically lysed by NK-92-scFv(FRP5)-ζ cells in comparison to parental NK-92 cells. At the effector to target ratio of 10:1 the specific lysis caused by NK-92-scFv(FRP5)-ζ cells is higher than that caused by parental NK-cells but not significantly so. A higher effector to target ratio would have to be tested to assess the significance of the result. In addition, labeled NK-92-scFv(FRP5)-ζ cells do not specifically lyse ErbB2-expressing MCF-7 cells in comparison to labeled parental NK-92 cells.

Control experiments showed that the same EpCAM-expressing tumor cells (DU-145, PC-3 and LNCaP) or ErbB2-expressing breast cancer cells (MDA-MB-453)

were resistant to parental non-EpCAM-targeted or non-ErbB2-targeted NK-92 cells. Fig. 4.29 to 4.32 show the preservation of cytotoxicity after labeling NK cells with ferumoxides. Therefore unspecific parental NK-92 cells, ErbB2-specific NK-92-scFv(FRP5)-ζ cells, ErbB2-specific NK-92-scFv(FRP5)-mζ cells and EpCAM-specific NK-92-scFv(MOC31)-ζ were labeled with ferumoxides before incubation with K562 cells as targets. Cytotoxic activity of unlabeled parental NK-92 cells, NK-92-scFv(FRP5)-ζ cells, NK-92-scFv(FRP5)-mζ cells and NK-92-scFv(MOC31)-ζ cells are shown for comparison. The cytotoxicity was not affected by labeling the cells.

For the in vivo assay the NK cell line NK-92-scFv(MOC31)-ζ and the prostate cancer cell line DU-145 cells were used. The accumulation of DID-labeled NK cells in the prostate cancers could be tracked in vivo with optical imaging. After their intravenous injection into athymic nude rats DID-labeled NK-92-scFv(MOC31)-ζ cells that express a chimeric receptor against the EpCAM antigen could be tracked to EpCAM-expressing DU-145 prostate cancers. In contrast to this, DID-labeled parental NK-92 cells could not be tracked to EpCAM-positive DU-145 prostate cancers.

As NK cells supply a high specificity of target cell recognition, a deficiency of inhibitory receptors, enhanced cytotoxicity against malignant cells as well as low toxicity against non-malignant cells, the investigation of tumor therapies with NK cells is strongly encouraged in preclinical and initial clinical trials [99, 106]. However, it is documented that various NK cell populations and tumor types differ in the extent of cytotoxicity [106]. The non-invasive optical imaging technique of tracking NK cells described in this thesis could be put to use for preclinical evaluation of these new immunotherapies. Furthermore it could improve the development of cognate clinical trials.

The experiments documented in this thesis show for the first time an in vivo tracking of DID-labeled NK cells to prostate carcinoma by fluorescence imaging. OI has many advantages over other imaging techniques including speed, no irradiation exposure and molecular sensitivity; it is nontoxic, reproducible and inexpensive [63, 118, 125]. However, there are studies with bioluminescent imaging for NK cell tracking [32, 41]. An example of bioluminescent imaging is the tracking of cytokine-induced NK cells that express luc to subcutaneous

tumors [28]. Although bioluminescent imaging provides a higher sensitivity compared to optical imaging the disadvantages outweigh the advantages: the methods for transduction are more expensive and the risk of immunogenicity is increased through the application of the fusion proteins. Even MRI was applied for tracking genetically engineered NK-92-scFv(FRP5)-ζ cells to HER2/neu-positive breast cancers [18]. MR imaging has the distinct advantage of providing a high soft tissue contrast (< 1 mm in plane) and is not associated with any irradiation exposure. MR imaging provides several advantages for the tracking of NK-cell immunotherapy, including three-dimensional data with high anatomical resolution, well-defined soft tissue contrast and no irradiation to the cells or the patient. Disadvantages of MR compared to optical or radiotracer based imaging techniques include limited sensitivity and expensive equipment which limits close follow up studies. A large number of variable parameters affect the sensitivity of the MR technique, such as field strength, pulse sequence parameters and the nature of coils being utilized [5, 6, 13, 20, 35, 43, 66, 116]. Techniques to track indium 111–oxine-labeled leukocytes are established in clinical practice, especially for the detection of inflammation [104]. These techniques are applicable in a clinical environment, but are not used for NK cell tracking. For tracking immune cells like T lymphocytes, dendritic cells or monoctyes, to fibrosarcoma, glioma, lymphoma or colon carcinoma, other imaging modalities such as PET and SPECT are used [2, 65, 78]. The advantage of these modalities is that they are ready for clinical use; however, they are expensive and associated with radiation exposure and decay of the label.

As previously mentioned, two different cell labeling assays were performed in this thesis. In order to verify the cytotoxicity of labeled NK cells in vitro the ferumoxide Endorem was used for the application of MR Imaging. In vivo studies with MRI were beyond the scope of this thesis. For the in vivo study, cells were labeled with DiD. The described protocol provides effective NK cell labeling by simple incubation with a commercially available NIR lipophilic dye for a few minutes. The advantage of this technique is the lower complexity and lower cost relative to previously applied labeling techniques with radionuclides

[76, 87, 107], magnetic resonance agents [18, 42, 47], bio-luminescent labels [1, 103] or reporter genes [15, 41, 89].

Adoptive immunotherapy is an innovative and promising approach in the treatment of cancer and is based on the idea of destroying malignancy by a stimulated immune system. It offers a new treatment option for patients with prostate cancer that is hormone-refractory. This stage is difficult to control and impossible to cure with standard chemotherapy regimens. Therefore the NK cells need to be targeted to the EpCAM-antigens on prostate cancer cells. Previous investigations of adoptive immunotherapies or EpCAM-targeted antibody therapies have been performed in prostate cancers [8, 29, 70, 99, 105]. However, to the best of our knowledge, the approach of the UCSF research group documented in this thesis is the first study that combines these two approaches.

Immunotherapies used for prostate cancer imply cellular immunotherapy with CD8+ T lymphocytes which are directed to the EpCAM-antigen [29] and dendritic cell–mediated vaccination therapy [70, 105]. Arnon et al. recently submitted a publication for the treatment of the prostate cancer cell lines DU145 and PC3 in vivo. They used NKp30-Ig that consists of a natural cytotoxic receptor fused with human IgG1 directed against the antigens on the prostate cancer cells [8].

The NK-92 cell line examined in our in vivo OI study has been previously used for adoptive immunotherapy of breast carcinoma, ovarian carcinoma, myeloma, and leukemia; however, it has not yet been used for prostate cancer [69, 99, 110]. A key benefit of NK cell therapy in comparison to other immunotherapy approaches is that the effect of cytotoxicity is stronger and NK cell therapy is not immunogenic [106].

As 87% of human prostate cancers demonstrate a large amount of EpCAM expression and thus EpCAM-negative prostate cancers are rare, prostate cancer immunotherapy focuses on the EpCAM-antigen. Additionally the antigen expression does not fluctuate significantly with different tumor grades or histopathologies [120].

However, tissues of other organs can be affected by genetically modified NK cells as EpCAM is expressed in various epithelial tissues as for instance in the

pancreas, jejunum, colon, kidney and salivary glands. Anti-EpCAM Ag immunotherapy has achieved phase II clinical trials in patients with prostate cancers as the toxicity of EpCAM-specific antibodies in humans is considered acceptable. Therapy protocols that were recently submitted include ING-1 [23], adecatumumab [71, 79], edrecolomab and an anti-EpCAM-directed immunotoxin [25, 128]. Kosterink et al. characterized an EpCAM transgenic mouse tumor model in order to explore the effects of anti-EpCAM-directed immunotherapy [51].

This thesis outlines the combination of NK cell immunotherapy and EpCAM-directed therapy as genetically modified NK-92-scFv(MOC31)-ζ cells that express a chimeric antigen receptor specific for the EpCAM-antigen are examined [119]. Suck et al. showed that the immunotherapy approach with modified NK cells that are directed to tumors supply a highly efficient tumor cell lysis in other types of cancers, such as breast cancers, ovarian cancers, leukemia, and myeloma [99]. The cytotoxicity assays used in this thesis demonstrate an effective cytolysis of EpCAM-expressing DU-145 prostate cancer cells by EpCAM-targeted NK-92-scFv(MOC31)-ζ cells.

As modified NK cells are equipped with built-in antibody-dependent cell-mediated cytotoxicity (ADCC), it is advantageous to use these cells since the killing of their targets proceeds regardless of endogenous immune effector mechanisms. This means that features of the host immune system are not needed for the cells to be effective. The cells ought to behave equally both in immunocompetent hosts and in immunodeficient animals. However, it should be noted that antibody and T-cell responses of the host immune system may develop against the NK cells if these cells are used as allogenic cells in humans and in this way limit the time period in which they can be used. This issue should be examined in further detail in future studies in immunocompetent animals and in clinical trials in humans.

There are several limitations of the in vitro and the in vivo studies analyzed in this thesis. Concerning the in vitro study, MCF-7 cells are not specifically lysed by labeled or unlabeled NK-92-scFv(FRP5)-ζ cells in comparison to parental NK-92 cells. Therefore these assays have to be repeated. The K562-assays showed that the cytotoxicity was not affected by labeling the NK cells. However,

the cytotoxicity has to be verified for each NK cell line when labeled. As regards the in vivo analysis, a limited number of animals (12) was used to obtain statistical significance. In order to confirm a superior tumor recognition of NK-92-scFv(MOC31)-ζ cells compared to parental NK-92 cells with optical imaging technique, power calculations determined a required minimal number of six animals per experimental group. A larger sample size would provide further characterization of interindividual and intraindividual variations of the acquired data. Furthermore, for the in vivo study the human DU-145 prostate cancer cell line was used since DU-145 demonstrates high EpCAM expression and can be grown as xenografts in athymic nude rats. The other two human prostate cancer cell lines LnCAP and PC-3 included in the in vitro component of this thesis have to be evaluated in the efficacy of the immunotherapy and imaging technique as LnCAP demonstrates higher and PC-3 lower levels of EpCAM expression [102]. Lastly human prostate cancers and human NK cells were examined in a xenograft animal model. While this imaging technique has potential clinical applications, the technique encounters several challenges for translational applications. DiD was chosen for this study as the cell labeling is fast and simple to accomplish without affecting NK cell function. The dye is visualized with the Cy5 filter of the fluorescence microscope and thus histopathologic results could be confirmed. The fluorochrome DiD has not received Food and Drug Administration (FDA) approval. However, another cyanine fluorescent dye, Indocyanine Green (ICG), has received FDA-approval. Since ICG demonstrates a high excitation and emission wavelength, comparative studies with standard fluorescence microscopy are limited, as lower wavelengths are needed. Additionally the limited penetration depth of fluorescence reflectance imaging restricts the clinical application of this technique; but there are several recent developments of tomographic fluorescence systems which could solve this problem.

In conclusion, the development of new immunotherapies for prostate cancer treatment is imperative as this type of tumor is frequent, EpCAM-positive and does not typically respond to conventional chemotherapy. The presented NK cell therapy with noninvasive imaging techniques for in vivo depiction and tracking of NK cells is important for the advancement of new treatment options.

The data presented in this thesis demonstrate that optical imaging can determine the presence and time point of NK cell accumulation in prostate cancers. Protocol optimizations for the preclinical treatment could make the application of this OI-based NK cell tracking technique possible. Several studies have to be performed, such as comparative investigations of the in vivo spreading and tumor accumulation of different NK cell types, comparisons between NK cells and immune cells such as dendritic cells or T lymphozytes. Moreover tests of the potency of these immune cells against different tumor types, androgen receptor-positive and –negative types have to be pursued. Further studies should also assess the effect of various combination therapies.

6 Summary

The purpose of this thesis was to confirm the cytotoxicity of genetically modified natural killer cells in comparison to non-targeted natural killer cells, unlabeled or ferumoxide labeled, and to track fluorophore-labeled (DiD), tumor-targeted natural killer cells to human prostate tumors with optical imaging.

The data collected in this thesis demonstrate the specificity of target cell recognition and enhanced cytotoxicity of genetically modified NK cells in various in vitro cytotoxicity assays. Several flow cytometry–based cytotoxicity assays were performed for both prostate and breast cancer cell lines: the specific cell killing of NK-92-scFv(MOC31)-ζ or NK-92-scFv(FRP5)-mζ cells towards the prostate cancer cell lines DU-145, PC-3 and LNCaP were tested as well as the specific cell killing of NK-92-scFv(FRP5)-ζ cells towards the breast cancer cell lines MDA-MB-453 and MCF-7. For each prostate or breast cancer cell line the unspecific cell killing of non-targeted parental NK-92 was tested in comparison. For the in vitro part of this thesis a labeling assay was performed as well; NK-92-scFv(FRP5)-ζ cells were labeled with the ferumoxide Endorem and the specific cell killing of these labeled cells was tested towards MCF-7. The unspecific cell killing of labeled NK-92 cells was tested in comparison. The preservation of cytotoxicity after labeling NK cells with ferumoxides was demonstrated by labeling assays with the reference cell K562. Unspecific parental NK-92 cells, ErbB2-specific NK-92-scFv(FRP5)-ζ cells, ErbB2-specific NK-92-scFv(FRP5)-mζ cells and EpCAM-specific NK-92-scFv(MOC31)-ζ were labeled with the ferumoxide Endorem before incubation with K562 cells as targets. Cytotoxic activity of unlabeled parental NK-92 cells, NK-92-scFv(FRP5)-ζ cells, NK-92-scFv(FRP5)-mζ and NK-92-scFv(MOC31)-ζ cells were shown for comparison. The Trypan Blue Test was used to determine the viability of cells. The Prussian Blue Test confirmed the intracellular presence of

the iron-containing contrast agent. The cell-surface expression of the chimeric antigen receptors scFv(FRP5)-ζ, scFv(FRP5)-mζ or scFv(MOC31)-ζ was determined by fluorescence activated cell sorter (FACS) analysis.

The in vivo assay used the parental NK cell line NK-92, the genetically modified NK cell line NK-92-scFv(MOC31)-ζ and the prostate cancer cell line DU-145. DiD-labeled parental NK-92 cells or DiD-labeled NK-92-scFv(MOC31)-ζ cells were injected intravenously into 12 athymic nude rats with implanted prostate cancer. OI scans were performed before and up to 24 hours postinjection. The tumor fluorescence intensity was determined and compared between pre- and postinjection scans and between the two cohorts using t-tests. Fluorescence microscopy was conducted in order to confirm the accumulation of DiD-labeled NK-92-scFv(MOC31)-ζ cells in the tumors at 24 hours post injection in comparison to the absence of parental NK-92 cells in the tumors. A significant increase in tumor fluorescence at 24 hours post injection of tumor-targeted NK-92-scFv(MOC31)-ζ cells was observed in contrast to parental NK-92 cells. The specific accumulation of NK-92-scFv(MOC31)-ζ cells was verified in the ex vivo OI scans and fluorescence microscopy. Parental NK-92 cells were not detectable in the tumors.

EpCAM-targeted DiD-labeled NK-92-scFv(MOC31)-ζ cells were tracked to prostate cancers with optical imaging.

7 Zusammenfassung

Ziel dieser Doktorarbeit war, die Zytotoxizität genetisch modifizierter T-Lymphozyten (natürliche Killerzellen) im Vergleich zu nicht Tumor gerichteten natürlichen Killerzellen in vitro, die entweder nicht markiert oder mit Eisenoxiden markiert waren, zu bestätigen und die Akkumulation intravenös injizierter, mit Fluorophore (DiD) markierter zytotoxischer T-Lymphozyten in EpCAM-positiven Prostatatumoren mittels Optical Imaging nachzuweisen.

In unterschiedlichen in vitro-Experimenten wurde die spezifische Zellerkennung und die gesteigerte Zytotoxizität der genetisch modifizierten T-Lymphozyten bewiesen. Folgende Zytotoxizitätsversuche mit Prostata- und Brustkrebszelllinien wurden mittels Durchflusszytometrie (FACS) durchgeführt: die Prostatazelllinien DU-145, PC-3 und LNCaP wurden mit genetisch modifizierten NK-92-scFv(MOC31)-ζ bzw. NK-92-scFv(FRP5)-mζ-Zellen auf spezifische Zelllysierung getestet. Ebenso wurden identische Tests mit den Brustkrebszellen MDA-MB-453 und MCF-7 mit NK-92-scFv(FRP5)-ζ durchgeführt. Zum Vergleich wurde die unspezifische Zelllyse von nicht modifizierten NK-92-Zellen gegen die verschiedenen Prostata- bzw. Brustkrebszellen getestet. Im Anschluss wurden NK-92-scFv(FRP5)-ζ-Zellen mit dem Eisenoxid Endorem markiert und die spezifische Zelllyse gegen die Brustkrebszelllinie MCF-7 getestet. Zum Vergleich wurden nicht Tumor gerichtete NK-92-Zellen markiert und ebenfalls getestet. Markierungsexperimente mit der Referenzzelllinie K562 zeigten den Erhalt der Zytotoxizität der NK-Zellen nach Markierung mit Eisenoxiden. Nicht Tumor gerichtete NK-92-, ErbB2-positive NK-92-scFv(FRP5)-ζ-, ErbB2-positive NK-92-scFv(FRP5)-mζ- und EpCAM-positive NK-92-scFv(MOC31)-ζ-Zellen wurden mit dem Eisenoxid Endorem markiert und mit den Zielzellen K562 inkubiert. Zum Vergleich wurde die zytotoxische Aktivität von nicht markierten NK-92-Zellen,

NK-92-scFv(FRP5)-ζ-, NK-92-scFv(FRP5)-mζ- und NK-92-scFv(MOC31)-ζ-Zellen aufgezeigt. Mit dem Trypanblau-Test wurde die Lebensfähigkeit der Zellen bestimmt. Die Berliner Blau Färbung bestätigte die Inkorporation der Eisenoxide in den Zellen. Die Durchflusszytometrie bewies die Expression der spezifischen chimären Antigenrezeptoren scFv(FRP5)-ζ, scFv(FRP5)-mζ, scFv(MOC31)-ζ auf der Zelloberfläche.

Für die in vivo Experimente wurden die natürliche Killerzelllinie, die genetisch modifizierte Zelllinie NK-92-scFv(MOC31)-ζ und die Prostatazelllinie DU-145 verwendet. 12 athymischen Nacktratten wurden EpCAM-positive Tumoren subkutan neben der Leber implantiert. Die Ratten wurden in zwei Kohorten aufgeteilt und erhielten entweder DiD markierte NK-92-Zellen oder DiD markierte NK-92-scFv(MOC31)-ζ-Zellen intravenös. Es wurden Optical Imaging Scans vor und bis zu 24 Stunden nach Injektion durchgeführt. Die Intensität der Tumorfluoreszenz der Scans vor und nach der Injektion wurde mit Hilfe von T-Tests verglichen, ebenso die Intensität der beiden Kohorten. Die Fluoreszenzmikroskopie 24 Stunden nach Injektion bestätigte die Akkumulation der DiD markierten NK-92-scFv(MOC31)-ζ-Zellen in den Tumoren im Vergleich zum Fehlen der nicht Tumor gerichteten NK-92-Zellen in den Tumoren. 24 Stunden nach der Injektion der genetisch modifizierten NK-92-scFv(MOC31)-ζ-Zellen konnte im Gegensatz zu den NK-92-Zellen ein signifikanter Anstieg der Tumorfluoreszenz festgestellt werden. Die spezifische Akkumulation der NK-92-scFv(MOC31)-ζ-Zellen wurde in den ex vivo Scans und in der Fluoreszenzmikroskopie bestätigt. Nicht Tumor gerichtete NK-92-Zellen konnten nicht in den Tumoren nachgewiesen werden.

DiD markierte NK-92-scFv(MOC31)-ζ-Zellen, die gegen das EpCAM-Antigen gerichtet sind, konnten mittels Optical Imaging zu Prostatatumoren verfolgt werden.

References

1. Adams, C.L., Kobets, N., Meiklejohn, G.R., Millington, O.R., Morton, A.M., Rush, C.M., Smith, K.M., Garside, P.
   Tracking lymphocytes in vivo
   Arch Immunol Ther Exp, 52 (2004) 173-187
2. Adonai, N., Nguyen, K.N., Walsh, J., Iyer, M., Toyokuni, T., Phelps, M.E., Mccarthy, T., Mccarthy, D.W., Gambhir, S.S.
   Ex vivo cell labeling with 64Cu-pyruvaldehyde-bis(N4-methylthiosemicarbazone) for imaging cell trafficking in mice with positron-emission tomography
   Proc Natl Acad Sci U S A, 99 (2002) 3030-3035
3. Alimirah, F., Chen, J., Basrawala, Z., Xin, H., Choubey, D.
   DU-145 and PC-3 human prostate cancer cell lines express androgen receptor: implications for the androgen receptor functions and regulation
   FEBS Lett, 580 (2006) 2294-2300
4. Arbab, A.S., Jordan, E.K., Wilson, L.B., Yocum, G.T., Lewis, B.K., Frank, J.A.
   In vivo trafficking and targeted delivery of magnetically labeled stem cells
   Hum Gene Ther, 15 (2004) 351-360
5. Arbab, A.S., Yocum, G.T., Kalish, H., Jordan, E.K., Anderson, S.A., Khakoo, A.Y., Read, E.J., Frank, J.A.
   Efficient magnetic cell labeling with protamine sulfate complexed to ferumoxides for cellular MRI
   Blood, 104 (2004) 1217-1223
6. Arbab, A.S., Yocum, G.T., Rad, A.M., Khakoo, A.Y., Fellowes, V., Read, E.J., Frank, J.A.

Labeling of cells with ferumoxides-protamine sulfate complexes does not inhibit function or differentiation capacity of hematopoietic or mesenchymal stem cells
NMR Biomed, 18 (2005) 553-559

7. Arlen, P.M., Dahut, W.L., Gulley, J.L.
Immunotherapy for prostate cancer: what's the future?
Hematol Oncol Clin North Am, 20 (2006) 965-983, xi

8. Arnon, T.I., Markel, G., Bar-Ilan, A., Hanna, J., Fima, E., Benchetrit, F., Galili, R., Cerwenka, A., Benharroch, D., Sion-Vardy, N., Porgador, A., Mandelboim, O.
Harnessing soluble NK cell killer receptors for the generation of novel cancer immune therapy
PLoS One, 3 (2008) e2150

9. Askenasy, N., Farkas, D.L.
Optical imaging of PKH-labeled hematopoietic cells in recipient bone marrow in vivo
Stem Cells, 20 (2002) 501-513

10. Balzar, M., Bakker, H.A., Briaire-De-Bruijn, I.H., Fleuren, G.J., Warnaar, S.O., Litvinov, S.V.
Cytoplasmic tail regulates the intercellular adhesion function of the epithelial cell adhesion molecule
Mol Cell Biol, 18 (1998) 4833-4843

11. Böcker, W., Denk, H., Heitz, P.U., Moch, H., Höfler, G., Kreipe, H.
"Pathologie"
Elsevier, Urban & Fischer, München, 2012,

12. Brinkley, B.R., Beall, P.T., Wible, L.J., Mace, M.L., Turner, D.S., Cailleau, R.M.
Variations in cell form and cytoskeleton in human breast carcinoma cells in vitro
Cancer Res, 40 (1980) 3118-3129

13. Bulte, J.W., Douglas, T., Witwer, B., Zhang, S.C., Strable, E., Lewis, B.K., Zywicke, H., Miller, B., Van Gelderen, P., Moskowitz, B.M., Duncan, I.D., Frank, J.A.

Magnetodendrimers allow endosomal magnetic labeling and in vivo tracking of stem cells
Nat Biotechnol, 19 (2001) 1141-1147

14. Bulte, J.W., Laughlin, P.G., Jordan, E.K., Tran, V.A., Vymazal, J., Frank, J.A.
Tagging of T cells with superparamagnetic iron oxide: uptake kinetics and relaxometry
Acad Radiol, 3 Suppl 2 (1996) S301-303

15. Cao, Y.A., Wagers, A.J., Beilhack, A., Dusich, J., Bachmann, M.H., Negrin, R.S., Weissman, I.L., Contag, C.H.
Shifting foci of hematopoiesis during reconstitution from single stem cells
Proc Natl Acad Sci U S A, 101 (2004) 221-226

16. Chan, Y.J., Chiou, C.J., Huang, Q., Hayward, G.S.
Synergistic interactions between overlapping binding sites for the serum response factor and ELK-1 proteins mediate both basal enhancement and phorbol ester responsiveness of primate cytomegalovirus major immediate-early promoters in monocyte and T-lymphocyte cell types
J Virol, 70 (1996) 8590-8605

17. Clark, R.E., Dodi, I.A., Hill, S.C., Lill, J.R., Aubert, G., Macintyre, A.R., Rojas, J., Bourdon, A., Bonner, P.L., Wang, L., Christmas, S.E., Travers, P.J., Creaser, C.S., Rees, R.C., Madrigal, J.A.
Direct evidence that leukemic cells present HLA-associated immunogenic peptides derived from the BCR-ABL b3a2 fusion protein
Blood, 98 (2001) 2887-2893

18. Daldrup-Link, H.E., Meier, R., Rudelius, M., Piontek, G., Piert, M., Metz, S., Settles, M., Uherek, C., Wels, W., Schlegel, J., Rummeny, E.J.
In vivo tracking of genetically engineered, anti-HER2/neu directed natural killer cells to HER2/neu positive mammary tumors with magnetic resonance imaging
Eur Radiol, 15 (2005) 4-13

19. Daldrup-Link, H.E., Rudelius, M., Metz, S., Piontek, G., Pichler, B., Settles, M., Heinzmann, U., Schlegel, J., Oostendorp, R.A., Rummeny, E.J.

Cell tracking with gadophrin-2: a bifunctional contrast agent for MR imaging, optical imaging, and fluorescence microscopy
Eur J Nucl Med Mol Imaging, 31 (2004) 1312-1321

20. Daldrup-Link, H.E., Rudelius, M., Oostendorp, R.A., Settles, M., Piontek, G., Metz, S., Rosenbrock, H., Keller, U., Heinzmann, U., Rummeny, E.J., Schlegel, J., Link, T.M.
Targeting of hematopoietic progenitor cells with MR contrast agents
Radiology, 228 (2003) 760-767

21. Daldrup-Link, H.E., Rudelius, M., Piontek, G., Metz, S., Brauer, R., Debus, G., Corot, C., Schlegel, J., Link, T.M., Peschel, C., Rummeny, E.J., Oostendorp, R.A.
Migration of iron oxide-labeled human hematopoietic progenitor cells in a mouse model: in vivo monitoring with 1.5-T MR imaging equipment
Radiology, 234 (2005) 197-205

22. Dawson, N.A.
New molecular targets in advanced prostate cancer
Expert Rev Anticancer Ther, 6 (2006) 993-1002

23. De Bono, J.S., Tolcher, A.W., Forero, A., Vanhove, G.F., Takimoto, C., Bauer, R.J., Hammond, L.A., Patnaik, A., White, M.L., Shen, S., Khazaeli, M.B., Rowinsky, E.K., Lobuglio, A.F.
ING-1, a monoclonal antibody targeting Ep-CAM in patients with advanced adenocarcinomas
Clin Cancer Res, 10 (2004) 7555-7565

24. De Vries, I.J., Lesterhuis, W.J., Barentsz, J.O., Verdijk, P., Van Krieken, J.H., Boerman, O.C., Oyen, W.J., Bonenkamp, J.J., Boezeman, J.B., Adema, G.J., Bulte, J.W., Scheenen, T.W., Punt, C.J., Heerschap, A., Figdor, C.G.
Magnetic resonance tracking of dendritic cells in melanoma patients for monitoring of cellular therapy
Nat Biotechnol, 23 (2005) 1407-1413

25. Di Paolo, C., Willuda, J., Kubetzko, S., Lauffer, I., Tschudi, D., Waibel, R., Pluckthun, A., Stahel, R.A., Zangemeister-Wittke, U.

A recombinant immunotoxin derived from a humanized epithelial cell adhesion molecule-specific single-chain antibody fragment has potent and selective antitumor activity
Clin Cancer Res, 9 (2003) 2837-2848

26. Doane, A.S., Danso, M., Lal, P., Donaton, M., Zhang, L., Hudis, C., Gerald, W.L.
An estrogen receptor-negative breast cancer subset characterized by a hormonally regulated transcriptional program and response to androgen
Oncogene, 25 (2006) 3994-4008

27. Ebina, T., Fujimiya, Y., Yamaguchi, T., Ogama, N., Sasaki, H., Isono, N., Suzuki, Y., Katakura, R., Tanaka, K., Nagata, K., Takano, S., Tamura, K., Uno, K., Kishida, T.
The use of BRM-activated killer cells in adoptive immunotherapy: a pilot study with nine advanced cancer patients
Biotherapy, 11 (1998) 241-253

28. Edinger, M., Cao, Y.A., Verneris, M.R., Bachmann, M.H., Contag, C.H., Negrin, R.S.
Revealing lymphoma growth and the efficacy of immune cell therapies using in vivo bioluminescence imaging
Blood, 101 (2003) 640-648

29. Elkord, E.
Immunology and immunotherapy approaches for prostate cancer
Prostate Cancer Prostatic Dis, 10 (2007) 224-236

30. Farag, S.S., Caligiuri, M.A.
Human natural killer cell development and biology
Blood Rev, 20 (2006) 123-137

31. Fawwaz, R.A., Oluwole, S., Wang, T.S., Kuromoto, N., Iga, C., Hardy, M.A., Alderson, P.O.
Biodistribution of radiolabeled lymphocytes
Radiology, 155 (1985) 483-486

32. Figdor, C.G., De Vries, I.J., Lesterhuis, W.J., Melief, C.J.
Dendritic cell immunotherapy: mapping the way
Nat Med, 10 (2004) 475-480

33. Frangioni, J.V., Hajjar, R.J.
In vivo tracking of stem cells for clinical trials in cardiovascular disease
Circulation, 110 (2004) 3378-3383

34. Frank, J.A., Anderson, S.A., Kalsih, H., Jordan, E.K., Lewis, B.K., Yocum, G.T., Arbab, A.S.
Methods for magnetically labeling stem and other cells for detection by in vivo magnetic resonance imaging
Cytotherapy, 6 (2004) 621-625

35. Frank, J.A., Miller, B.R., Arbab, A.S., Zywicke, H.A., Jordan, E.K., Lewis, B.K., Bryant, L.H., Jr., Bulte, J.W.
Clinically applicable labeling of mammalian and stem cells by combining superparamagnetic iron oxides and transfection agents
Radiology, 228 (2003) 480-487

36. Franke-Fayard, B., Waters, A.P., Janse, C.J.
Real-time in vivo imaging of transgenic bioluminescent blood stages of rodent malaria parasites in mice
Nat Protoc, 1 (2006) 476-485

37. Gheysens, O., Lin, S., Cao, F., Wang, D., Chen, I.Y., Rodriguez-Porcel, M., Min, J.J., Gambhir, S.S., Wu, J.C.
Noninvasive evaluation of immunosuppressive drug efficacy on acute donor cell survival
Mol Imaging Biol, 8 (2006) 163-170

38. Haas, G.P., Delongchamps, N., Brawley, O.W., Wang, C.Y., De La Roza, G.
The worldwide epidemiology of prostate cancer: perspectives from autopsy studies
Can J Urol, 15 (2008) 3866-3871

39. Hadjantonakis, A.K., Papaioannou, V.E.
Dynamic in vivo imaging and cell tracking using a histone fluorescent protein fusion in mice
BMC Biotechnol, 4 (2004) 33

40. Hallett, W.H., Murphy, W.J.
Natural killer cells: biology and clinical use in cancer therapy

Cell Mol Immunol, 1 (2004) 12-21

41. Hardy, J., Edinger, M., Bachmann, M.H., Negrin, R.S., Fathman, C.G., Contag, C.H.
Bioluminescence imaging of lymphocyte trafficking in vivo
Exp Hematol, 29 (2001) 1353-1360

42. Hildebrandt, I.J., Gambhir, S.S.
Molecular imaging applications for immunology
Clin Immunol, 111 (2004) 210-224

43. Hoehn, M., Kustermann, E., Blunk, J., Wiedermann, D., Trapp, T., Wecker, S., Focking, M., Arnold, H., Hescheler, J., Fleischmann, B.K., Schwindt, W., Buhrle, C.
Monitoring of implanted stem cell migration in vivo: a highly resolved in vivo magnetic resonance imaging investigation of experimental stroke in rat
Proc Natl Acad Sci U S A, 99 (2002) 16267-16272

44. Hope-Ross, M., Yannuzzi, L.A., Gragoudas, E.S., Guyer, D.R., Slakter, J.S., Sorenson, J.A., Krupsky, S., Orlock, D.A., Puliafito, C.A.
Adverse reactions due to indocyanine green
Ophthalmology, 101 (1994) 529-533

45. Jeffery, D.A., Bogyo, M.
Chemical proteomics and its application to drug discovery
Curr Opin Biotechnol, 14 (2003) 87-95

46. Jung, C.W., Jacobs, P.
Physical and chemical properties of superparamagnetic iron oxide MR contrast agents: ferumoxides, ferumoxtran, ferumoxsil
Magn Reson Imaging, 13 (1995) 661-674

47. Kircher, M.F., Allport, J.R., Graves, E.E., Love, V., Josephson, L., Lichtman, A.H., Weissleder, R.
In vivo high resolution three-dimensional imaging of antigen-specific cytotoxic T-lymphocyte trafficking to tumors
Cancer Res, 63 (2003) 6838-6846

48. Klingemann, H.G.
Natural killer cell-based immunotherapeutic strategies

Cytotherapy, 7 (2005) 16-22

49. Koeffler, H.P., Golde, D.W.
Human myeloid leukemia cell lines: a review
Blood, 56 (1980) 344-350

50. Kokontis, J., Takakura, K., Hay, N., Liao, S.
Increased androgen receptor activity and altered c-myc expression in prostate cancer cells after long-term androgen deprivation
Cancer Res, 54 (1994) 1566-1573

51. Kosterink, J.G., Mclaughlin, P.M., Lub-De Hooge, M.N., Hendrikse, H.H., Van Zanten, J., Van Garderen, E., Harmsen, M.C., De Leij, L.F.
Biodistribution studies of epithelial cell adhesion molecule (EpCAM)-directed monoclonal antibodies in the EpCAM-transgenic mouse tumor model
J Immunol, 179 (2007) 1362-1368

52. Lacroix, M., Toillon, R.A., Leclercq, G.
p53 and breast cancer, an update
Endocr Relat Cancer, 13 (2006) 293-325

53. Lamb, D.J., Zhang, L.
Challenges in prostate cancer research: animal models for nutritional studies of chemoprevention and disease progression
J Nutr, 135 (2005) 3009S-3015S

54. Leemhuis, T., Wells, S., Scheffold, C., Edinger, M., Negrin, R.S.
A phase I trial of autologous cytokine-induced killer cells for the treatment of relapsed Hodgkin disease and non-Hodgkin lymphoma
Biol Blood Marrow Transplant, 11 (2005) 181-187

55. Levenson, A.S., Jordan, V.C.
MCF-7: the first hormone-responsive breast cancer cell line
Cancer Res, 57 (1997) 3071-3078

56. Lewin, M., Carlesso, N., Tung, C.H., Tang, X.W., Cory, D., Scadden, D.T., Weissleder, R.
Tat peptide-derivatized magnetic nanoparticles allow in vivo tracking and recovery of progenitor cells
Nat Biotechnol, 18 (2000) 410-414

57. Ley, C.D., Horsman, M.R., Kristjansen, P.E.
Early effects of combretastatin-A4 disodium phosphate on tumor perfusion and interstitial fluid pressure
Neoplasia, 9 (2007) 108-112

58. Li, H., Cao, M.Y., Lee, Y., Lee, V., Feng, N., Benatar, T., Jin, H., Wang, M., Der, S., Wright, J.A., Young, A.H.
Virulizin, a novel immunotherapy agent, activates NK cells through induction of IL-12 expression in macrophages
Cancer Immunol Immunother, 54 (2005) 1115-1126

59. Licha, K., Olbrich, C.
Optical imaging in drug discovery and diagnostic applications
Adv Drug Deliv Rev, 57 (2005) 1087-1108

60. Ligeza, J., Klein, A.
Growth factor/growth factor receptor loops in autocrine growth regulation of human prostate cancer DU145 cells
Acta Biochim Pol, 58 (2011) 391-396

61. Linja, M.J., Savinainen, K.J., Saramaki, O.R., Tammela, T.L., Vessella, R.L., Visakorpi, T.
Amplification and overexpression of androgen receptor gene in hormone-refractory prostate cancer
Cancer Res, 61 (2001) 3550-3555

62. Lozzio, C.B., Lozzio, B.B.
Human chronic myelogenous leukemia cell-line with positive Philadelphia chromosome
Blood, 45 (1975) 321-334

63. Lucignani, G., Ottobrini, L., Martelli, C., Rescigno, M., Clerici, M.
Molecular imaging of cell-mediated cancer immunotherapy
Trends Biotechnol, 24 (2006) 410-418

64. Mcleskey, S.W., Ding, I.Y., Lippman, M.E., Kern, F.G.
MDA-MB-134 breast carcinoma cells overexpress fibroblast growth factor (FGF) receptors and are growth-inhibited by FGF ligands
Cancer Res, 54 (1994) 523-530

65. Melder, R.J., Brownell, A.L., Shoup, T.M., Brownell, G.L., Jain, R.K.

Imaging of activated natural killer cells in mice by positron emission tomography: preferential uptake in tumors
Cancer Res, 53 (1993) 5867-5871

66. Metz, S., Bonaterra, G., Rudelius, M., Settles, M., Rummeny, E.J., Daldrup-Link, H.E.
Capacity of human monocytes to phagocytose approved iron oxide MR contrast agents in vitro
Eur Radiol, 14 (2004) 1851-1858

67. Modo, M., Cash, D., Mellodew, K., Williams, S.C., Fraser, S.E., Meade, T.J., Price, J., Hodges, H.
Tracking transplanted stem cell migration using bifunctional, contrast agent-enhanced, magnetic resonance imaging
Neuroimage, 17 (2002) 803-811

68. Moore, A., Grimm, J., Han, B., Santamaria, P.
Tracking the recruitment of diabetogenic CD8+ T-cells to the pancreas in real time
Diabetes, 53 (2004) 1459-1466

69. Muller, T., Uherek, C., Maki, G., Chow, K.U., Schimpf, A., Klingemann, H.G., Tonn, T., Wels, W.S.
Expression of a CD20-specific chimeric antigen receptor enhances cytotoxic activity of NK cells and overcomes NK-resistance of lymphoma and leukemia cells
Cancer Immunol Immunother, 57 (2008) 411-423

70. Murphy, G., Tjoa, B., Ragde, H., Kenny, G., Boynton, A.
Phase I clinical trial: T-cell therapy for prostate cancer using autologous dendritic cells pulsed with HLA-A0201-specific peptides from prostate-specific membrane antigen
Prostate, 29 (1996) 371-380

71. Naundorf, S., Preithner, S., Mayer, P., Lippold, S., Wolf, A., Hanakam, F., Fichtner, I., Kufer, P., Raum, T., Riethmuller, G., Baeuerle, P.A., Dreier, T.
In vitro and in vivo activity of MT201, a fully human monoclonal antibody for pancarcinoma treatment

Int J Cancer, 100 (2002) 101-110

72. Niu, Y., Yeh, S., Miyamoto, H., Li, G., Altuwaijri, S., Yuan, J., Han, R., Ma, T., Kuo, H.C., Chang, C.
Tissue prostate-specific antigen facilitates refractory prostate tumor progression via enhancing ARA70-regulated androgen receptor transactivation
Cancer Res, 68 (2008) 7110-7119

73. Olayioye, M.A.
Update on HER-2 as a target for cancer therapy: intracellular signaling pathways of ErbB2/HER-2 and family members
Breast Cancer Res, 3 (2001) 385-389

74. Oostendorp, R.A., Ghaffari, S., Eaves, C.J.
Kinetics of in vivo homing and recruitment into cycle of hematopoietic cells are organ-specific but CD44-independent
Bone Marrow Transplant, 26 (2000) 559-566

75. Ormo, M., Cubitt, A.B., Kallio, K., Gross, L.A., Tsien, R.Y., Remington, S.J.
Crystal structure of the Aequorea victoria green fluorescent protein
Science, 273 (1996) 1392-1395

76. Paik, J.Y., Lee, K.H., Byun, S.S., Choe, Y.S., Kim, B.T.
Use of insulin to improve [18 F]fluorodeoxyglucose labelling and retention for in vivo positron emission tomography imaging of monocyte trafficking
Nucl Med Commun, 23 (2002) 551-557

77. Pinthus, J.H., Waks, T., Kaufman-Francis, K., Schindler, D.G., Harmelin, A., Kanety, H., Ramon, J., Eshhar, Z.
Immuno-gene therapy of established prostate tumors using chimeric receptor-redirected human lymphocytes
Cancer Res, 63 (2003) 2470-2476

78. Pittet, M.J., Grimm, J., Berger, C.R., Tamura, T., Wojtkiewicz, G., Nahrendorf, M., Romero, P., Swirski, F.K., Weissleder, R.
In vivo imaging of T cell delivery to tumors after adoptive transfer therapy
Proc Natl Acad Sci U S A, 104 (2007) 12457-12461

79. Prang, N., Preithner, S., Brischwein, K., Goster, P., Woppel, A., Muller, J., Steiger, C., Peters, M., Baeuerle, P.A., Da Silva, A.J.
Cellular and complement-dependent cytotoxicity of Ep-CAM-specific monoclonal antibody MT201 against breast cancer cell lines
Br J Cancer, 92 (2005) 342-349

80. Prikler, L., Scandella, E., Men, Y., Engeler, D.S., Diener, P.A., Gillessen, S., Ludewig, B., Schmid, H.P.
[Adaptive immunotherapy of the advanced prostate cancer - cancer testis antigen (CTA) as possible target antigens]
Aktuelle Urol, 35 (2004) 326-330

81. Pulukuri, S.M., Gondi, C.S., Lakka, S.S., Jutla, A., Estes, N., Gujrati, M., Rao, J.S.
RNA interference-directed knockdown of urokinase plasminogen activator and urokinase plasminogen activator receptor inhibits prostate cancer cell invasion, survival, and tumorigenicity in vivo
J Biol Chem, 280 (2005) 36529-36540

82. Quinn, M., Babb, P.
Patterns and trends in prostate cancer incidence, survival, prevalence and mortality. Part II: individual countries
BJU Int, 90 (2002) 174-184

83. Raju, B., Haug, S.R., Ibrahim, S.O., Heyeraas, K.J.
High interstitial fluid pressure in rat tongue cancer is related to increased lymph vessel area, tumor size, invasiveness and decreased body weight
J Oral Pathol Med, 37 (2008) 137-144

84. Raulet, D.H., Vance, R.E., Mcmahon, C.W.
Regulation of the natural killer cell receptor repertoire
Annu Rev Immunol, 19 (2001) 291-330

85. Reimer, P., Marx, C., Rummeny, E.J., Muller, M., Lentschig, M., Balzer, T., Dietl, K.H., Sulkowski, U., Berns, T., Shamsi, K., Peters, P.E.
SPIO-enhanced 2D-TOF MR angiography of the portal venous system: results of an intraindividual comparison
J Magn Reson Imaging, 7 (1997) 945-949

86. Rice, B.W., Cable, M.D., Nelson, M.B.

In vivo imaging of light-emitting probes
J Biomed Opt, 6 (2001) 432-440

87. Ridolfi, R., Riccobon, A., Galassi, R., Giorgetti, G., Petrini, M., Fiammenghi, L., Stefanelli, M., Ridolfi, L., Moretti, A., Migliori, G., Fiorentini, G.
Evaluation of in vivo labelled dendritic cell migration in cancer patients
J Transl Med, 2 (2004) 27

88. Rosenberg, S.
Lymphokine-activated killer cells: a new approach to immunotherapy of cancer
J Natl Cancer Inst, 75 (1985) 595-603

89. Schimmelpfennig, C.H., Schulz, S., Arber, C., Baker, J., Tarner, I., Mcbride, J., Contag, C.H., Negrin, R.S.
Ex vivo expanded dendritic cells home to T-cell zones of lymphoid organs and survive in vivo after allogeneic bone marrow transplantation
Am J Pathol, 167 (2005) 1321-1331

90. Schlemmer, H.P.
[Prostate carcinoma.]
Radiologe, 48 (2008) 45-51

91. Schoepf, U., Marecos, E.M., Melder, R.J., Jain, R.K., Weissleder, R.
Intracellular magnetic labeling of lymphocytes for in vivo trafficking studies
Biotechniques, 24 (1998) 642-646, 648-651

92. Shagin, D.A., Barsova, E.V., Yanushevich, Y.G., Fradkov, A.F., Lukyanov, K.A., Labas, Y.A., Semenova, T.N., Ugalde, J.A., Meyers, A., Nunez, J.M., Widder, E.A., Lukyanov, S.A., Matz, M.V.
GFP-like proteins as ubiquitous metazoan superfamily: evolution of functional features and structural complexity
Mol Biol Evol, 21 (2004) 841-850

93. Shah, K., Weissleder, R.
Molecular optical imaging: applications leading to the development of present day therapeutics
NeuroRx, 2 (2005) 215-225

94. Shaner, N.C., Campbell, R.E., Steinbach, P.A., Giepmans, B.N., Palmer, A.E., Tsien, R.Y.
Improved monomeric red, orange and yellow fluorescent proteins derived from Discosoma sp. red fluorescent protein
Nat Biotechnol, 22 (2004) 1567-1572

95. Shaner, N.C., Patterson, G.H., Davidson, M.W.
Advances in fluorescent protein technology
J Cell Sci, 120 (2007) 4247-4260

96. Shi, M., Zhang, B., Tang, Z.R., Lei, Z.Y., Wang, H.F., Feng, Y.Y., Fan, Z.P., Xu, D.P., Wang, F.S.
Autologous cytokine-induced killer cell therapy in clinical trial phase I is safe in patients with primary hepatocellular carcinoma
World J Gastroenterol, 10 (2004) 1146-1151

97. Speers, A.E., Cravatt, B.F.
Chemical strategies for activity-based proteomics
Chembiochem, 5 (2004) 41-47

98. Spitzweg, C., Zhang, S., Bergert, E.R., Castro, M.R., Mciver, B., Heufelder, A.E., Tindall, D.J., Young, C.Y., Morris, J.C.
Prostate-specific antigen (PSA) promoter-driven androgen-inducible expression of sodium iodide symporter in prostate cancer cell lines
Cancer Res, 59 (1999) 2136-2141

99. Suck, G.
Novel approaches using natural killer cells in cancer therapy
Semin Cancer Biol, 16 (2006) 412-418

100. Sundstrom, J.B., Mao, H., Santoianni, R., Villinger, F., Little, D.M., Huynh, T.T., Mayne, A.E., Hao, E., Ansari, A.A.
Magnetic resonance imaging of activated proliferating rhesus macaque T cells labeled with superparamagnetic monocrystalline iron oxide nanoparticles
J Acquir Immune Defic Syndr, 35 (2004) 9-21

101. Sutton, E.J., Henning, T.D., Pichler, B.J., Bremer, C., Daldrup-Link, H.E.
Cell tracking with optical imaging
Eur Radiol, 18 (2008) 2021-2032

102. Suzuki, K., Nakamura, K., Kato, K., Hamada, H., Tsukamoto, T.
Exploration of target molecules for prostate cancer gene therapy
Prostate, 67 (2007) 1163-1173

103. Sweeney, T.J., Mailander, V., Tucker, A.A., Olomu, A.B., Zhang, W., Cao, Y., Negrin, R.S., Contag, C.H.
Visualizing the kinetics of tumor-cell clearance in living animals
Proc Natl Acad Sci U S A, 96 (1999) 12044-12049

104. Takahashi, K., Ohyanagi, M., Ikeoka, K., Masai, M., Naruse, H., Iwasaki, T., Fukuchi, M., Miyamoto, T.
Detection of inflammation in aortic aneurysms with indium 111-oxine--labeled leukocyte imaging
J Nucl Cardiol, 8 (2001) 165-170

105. Tjoa, B.A., Simmons, S.J., Bowes, V.A., Ragde, H., Rogers, M., Elgamal, A., Kenny, G.M., Cobb, O.E., Ireton, R.C., Troychak, M.J., Salgaller, M.L., Boynton, A.L., Murphy, G.P.
Evaluation of phase I/II clinical trials in prostate cancer with dendritic cells and PSMA peptides
Prostate, 36 (1998) 39-44

106. Tonn, T., Becker, S., Esser, R., Schwabe, D., Seifried, E.
Cellular immunotherapy of malignancies using the clonal natural killer cell line NK-92
J Hematother Stem Cell Res, 10 (2001) 535-544

107. Trakatelli, M., Toungouz, M., Blocklet, D., Dodoo, Y., Gordower, L., Laporte, M., Vereecken, P., Sales, F., Mortier, L., Mazouz, N., Lambermont, M., Goldman, S., Coulie, P., Goldman, M., Velu, T.
A new dendritic cell vaccine generated with interleukin-3 and interferon-beta induces CD8+ T cell responses against NA17-A2 tumor peptide in melanoma patients
Cancer Immunol Immunother, 55 (2006) 469-474

108. Tung, C.H.
Fluorescent peptide probes for in vivo diagnostic imaging
Biopolymers, 76 (2004) 391-403

109. Uherek, C., Groner, B., Wels, W.

Chimeric antigen receptors for the retargeting of cytotoxic effector cells
J Hematother Stem Cell Res, 10 (2001) 523-534

110. Uherek, C., Tonn, T., Uherek, B., Becker, S., Schnierle, B., Klingemann, H.G., Wels, W.
Retargeting of natural killer-cell cytolytic activity to ErbB2-expressing cancer cells results in efficient and selective tumor cell destruction
Blood, 100 (2002) 1265-1273

111. Umekita, Y., Hiipakka, R.A., Kokontis, J.M., Liao, S.
Human prostate tumor growth in athymic mice: inhibition by androgens and stimulation by finasteride
Proc Natl Acad Sci U S A, 93 (1996) 11802-11807

112. Vuu, K., Xie, J., Mcdonald, M.A., Bernardo, M., Hunter, F., Zhang, Y., Li, K., Bednarski, M., Guccione, S.
Gadolinium-rhodamine nanoparticles for cell labeling and tracking via magnetic resonance and optical imaging
Bioconjug Chem, 16 (2005) 995-999

113. Wang, L., Jackson, W.C., Steinbach, P.A., Tsien, R.Y.
Evolution of new nonantibody proteins via iterative somatic hypermutation
Proc Natl Acad Sci U S A, 101 (2004) 16745-16749

114. Wang, Y.X., Hussain, S.M., Krestin, G.P.
Superparamagnetic iron oxide contrast agents: physicochemical characteristics and applications in MR imaging
Eur Radiol, 11 (2001) 2319-2331

115. Weissleder, R.
Liver MR imaging with iron oxides: toward consensus and clinical practice
Radiology, 193 (1994) 593-595

116. Weissleder, R., Cheng, H.C., Bogdanova, A., Bogdanov, A., Jr.
Magnetically labeled cells can be detected by MR imaging
J Magn Reson Imaging, 7 (1997) 258-263

117. Weissleder, R., Elizondo, G., Wittenberg, J., Rabito, C.A., Bengele, H.H., Josephson, L.

Ultrasmall superparamagnetic iron oxide: characterization of a new class of contrast agents for MR imaging
Radiology, 175 (1990) 489-493

118. Weissleder, R., Pittet, M.J.
Imaging in the era of molecular oncology
Nature, 452 (2008) 580-589

119. Wels, W., Biburger, M., Muller, T., Dalken, B., Giesubel, U., Tonn, T., Uherek, C.
Recombinant immunotoxins and retargeted killer cells: employing engineered antibody fragments for tumor-specific targeting of cytotoxic effectors
Cancer Immunol Immunother, 53 (2004) 217-226

120. Went, P., Vasei, M., Bubendorf, L., Terracciano, L., Tornillo, L., Riede, U., Kononen, J., Simon, R., Sauter, G., Baeuerle, P.A.
Frequent high-level expression of the immunotherapeutic target Ep-CAM in colon, stomach, prostate and lung cancers
Br J Cancer, 94 (2006) 128-135

121. Whiteside, T.L.
Immune cells in the tumor microenvironment. Mechanisms responsible for functional and signaling defects
Adv Exp Med Biol, 451 (1998) 167-171

122. Wilson, V.S., Bobseine, K., Lambright, C.R., Gray, L.E., Jr.
A novel cell line, MDA-kb2, that stably expresses an androgen- and glucocorticoid-responsive reporter for the detection of hormone receptor agonists and antagonists
Toxicol Sci, 66 (2002) 69-81

123. Wu, J.C., Chen, I.Y., Sundaresan, G., Min, J.J., De, A., Qiao, J.H., Fishbein, M.C., Gambhir, S.S.
Molecular imaging of cardiac cell transplantation in living animals using optical bioluminescence and positron emission tomography
Circulation, 108 (2003) 1302-1305

124. Xiong, T., Zhang, Z., Liu, B.F., Zeng, S., Chen, Y., Chu, J., Luo, Q.

In vivo optical imaging of human adenoid cystic carcinoma cell metastasis
Oral Oncol, 41 (2005) 709-715

125. Yang, X., Liu, H., Li, D., Zhou, X., Jung, W.C., Deans, A.E., Cui, Y., Cheng, L.
Digital optical imaging of green fluorescent proteins for tracking vascular gene expression: feasibility study in rabbit and human cell models
Radiology, 219 (2001) 171-175

126. Yeh, T.C., Zhang, W., Ildstad, S.T., Ho, C.
In vivo dynamic MRI tracking of rat T-cells labeled with superparamagnetic iron-oxide particles
Magn Reson Med, 33 (1995) 200-208

127. Zavattini, G., Vecchi, S., Mitchell, G., Weisser, U., Leahy, R.M., Pichler, B.J., Smith, D.J., Cherry, S.R.
A hyperspectral fluorescence system for 3D in vivo optical imaging
Phys Med Biol, 51 (2006) 2029-2043

128. Zimmermann, S., Wels, W., Froesch, B.A., Gerstmayer, B., Stahel, R.A., Zangemeister-Wittke, U.
A novel immunotoxin recognising the epithelial glycoprotein-2 has potent antitumoural activity on chemotherapy-resistant lung cancer
Cancer Immunol Immunother, 44 (1997) 1-9

List of Figures

List of Tables

Abbreviations

AKT	protein kinase B
ADCC	antibody-dependent cell-mediated cytotoxicity
A-NK	activated killer cells
AR	androgen receptor
CAM	cell adhesion receptors
CFSE	carboxyfluorescein succinimidyl ester
CCD camera	charge coupled device camera
DHT	dihydrotestosterone
DiD	1,19-dioctadecyl-3,3,39,39tetramethylindodicarbocyanine
DiI	1,1'-dioctadecyl-3,3,3',3'tetramethylindocarbocyanine-perchlorate
DiO	3,3'-dioctadecyloxacarbocyanineperchlorate
DMEM	modified eagle medium
DNA	deoxyribonucleic acid
EBV	Epstein–Barr virus
EDTA	ethylenediaminetetraacetic acid
E/F	effector to target ratio
e.g.	for example
EGF	epidermal growth factor
EPCAM	epithelial cell adhesion molecule
ErbB2	human epidermal growth factor receptor 2
ER	estrogen receptors
FACS	fluorescence activated cell sorter
FBS	fetal bovine serum
FDA	Food and Drug Administration
FGFR	fibroblast growth factor receptor
Fig	figure
FITC	fluorescein isothiocyanate
GFP	green fluorescent protein

ICG	indocyanine green
i.e.	that is
IGF	insulin-like growth factor
IL-2	interleukin-2
MHC	major histocompatibility complex
MRI	magnetic resonance imaging
mL	milliliter
µl	microliter
mAb	monoclonal antibody
NK cell	natural killer cell
NIR	near-infrared
OI	optical imaging
PBS	phosphate-buffered saline
PCR	polymerase chain reaction
PET	positron emission tomography
PI	propidium iodide
p.i.	post injection
RNA	ribonucleic acid
RPMI	Roswell Park Memorial Institute medium
ROI	regions-of-interest
Sc	single chain
SPECT	single-photon emission computed tomography
SPIO	superparamagnetic iron oxides
Tab	table
uPA	urokinase plasminogen activator
USPIO	ultrasmall paramagnetic iron oxides
UV	ultraviolet
VEGF	vascular endothelial growth factor

Acknowledgements

Herrn Univ.-Prof. Dr. Ernst J. Rummeny danke ich für die Übernahme der Arbeit an die radiologische Fakultät der Technischen Universität München.
Besonders möchte ich mich bei Frau Prof. Dr. Heike E. Daldrup-Link für die Bereitstellung des interessanten Themas, die herzliche Aufnahme in ihr Forschungsteam an der University of California San Francisco, die intensive Betreuung und vielseitige Unterstützung sowie für ihre wertvollen Ratschläge und Ideen, die zum Gelingen dieser Arbeit beigetragen haben, bedanken.
Herrn Prof. Dr. Wilfried Wels danke ich für die herzliche Aufnahme in seine Arbeitsgruppe im Chemotherapeutischen Forschungsinstitut Frankfurt am Main im Georg-Speyer-Haus. Bei Frau Christiane Knopp möchte ich mich für die hervorragende und kompetente Betreuung bedanken.
Herrn Sidhartha Tavri danke ich für die motivierende, herausragende und stets bereichernde Betreuung. Den weiteren Mitgliedern der Arbeitsgruppe von Frau Prof. Dr. Heike E. Daldrup-Link an der UCSF - Frau Priyanka Jha, Herrn Tobias Henning, Herrn Akilesh Sista und Frau Sophie Boddington - danke ich für die wertvollen Ratschläge und Hilfestellungen.
Herrn C. Uherek danke ich für die Bereitstellung der NK-92-Zellen.
Herrn Daniel Hostetter danke ich für die Hilfestellung bei der Fluorescence Microscopy.
Ein besonderer Dank gilt meiner Familie, die mich in jeder Hinsicht immer unterstützt hat.